Supporting Information for

Porous Silsesquioxane Imine Frameworks as Highly Efficient Adsorbents for Cooperative Iodine Capture

Mateusz Janeta,‡ Wojciech Bury,‡* Sławomir Szafert

[a] Faculty of Chemistry, University of Wrocław, 14 F. Joliot-Curie, 50-383 Wrocław, Poland

‡These authors contributed equally.

*Corresponding author: wojciech.bury@chem.uni.wroc.pl

Table of Contents

Section 1. Materials and Methods

Materials

Dimethyl sulfoxide (99.8% anhydrous, Aldrich) was dried over activated 4Å molecular sieves prior to use. Acetonitrile (99%, Chempur), benzene (99%, Aldrich), dichloromethane (99%, Chempur), chloroform (99%, Chempur), cyclohexane (99%, Chempur), ethanol (99%, J. T. Baker), hexane (99%, Chempur), mesitylene (99%, Aldrich), methanol (99%, J. T. Baker), chlorobenzene (99%, Aldrich), tetrahydrofuran (99%, Chempur), toluene (99%, Chempur), DMSO-d_6 (Cambridge Isotope, 99.9% D), $CDCl_3$ (Cambridge Isotope, 99% D), sulfuric acid-d_2 solution (Sigma Aldrich, 96-98 wt. % D_2SO_4, in D_2O, 99.5 atom % D), (3-aminopropyl)triethoxysilane (99%, Aldrich), triethylamine (99.5%, Aldrich), pyridinium chlorochromate (99%, Alfa Aesar), hexamethylenetetraamine (99%, Merck), 1,3,5-benzenetriol (99%, Aldrich), trifluoroacetic acid (99%, TCI), 4-formylphenylboronic acid (98%, Fluorochem), bis(triphenylphosphine)palladium(II) dichloride (≥99%, Aldrich), 1,3,5-tribromobenzene (99%, Fluorochem), HCl (36–38%, Chempur), K_2CO_3 (99%, Chempur), were used without further purification unless stated otherwise. All the gases used or the adsorption/desorption were ultra-high purity grade 5 and were obtained from Linde Gaz Polska (Kraków, Poland).

Chromium(III) acetylacetonate,[1] octa(3-aminopropyl)silsesquioxane hydrochloride,[1] compound **1**,[2] 2',5'-dimethyl-[1,1':4',1''-terphenyl]-4,4''-dicarbaldehyde,[3] 1,3,5-tris(hydroxy-methyl)benzene,[4] 1,3,5-benzenetricarbaldehyde,[4] 2,4,6-trihydroxybenzene-1,3,5-tricarbaldehyde[5,6] and 1,3,5-tris(4-formylphenyl)benzene,[7] were prepared by following the described procedure.

Characterization methods

^{1}H NMR and ^{13}C NMR spectra in solutions were recorded using a Bruker Avance 500 spectrometer equipped with broadband inverse gradient probe heads. Spectra were referred to the residual solvent signals ($(CD_3)_2SO$, 2.50; $CDCl_3$, 7.26; $(^{13}CH_3)_2SO$, 39.52; $^{13}CDCl_3$, 77.16 ppm) as an internal reference. For NMR sample preparation, a PSIF sample was dissolved in a few drops of D_2SO_4 by sonication. The obtained solution was then mixed with DMSO-d_6 and used for NMR measurement. ^{29}Si NMR spectra in solution were recorded on a Bruker AMX-300 spectrometer using Wilmad PTFE-FEP 5 mm tube liners. $Cr(acac)_3$ was added at a concentration of ~10^{-2} mol/L as a shiftless relaxation agent. Chemical shifts were referenced to TMS. ^{13}C cross-polarization, magic angle spinning (CP-MAS) nuclear magnetic resonance measurements were carried out on a Bruker AMX-300 spectrometer using a standard CP-MAS probe and 4 mm rotor with recycle delay for 10 s or a Bruker Avance III HD 600 MHz with 1.3

mm rotor with recycle delay for 5 s. All spectra were recorded at room temperature and referenced using adamantane peak at 38.5 ppm relative to TMS (run separately). ^{29}Si and ^{15}N CP-MAS NMR spectra were measured on a Bruker Avance III HD 600 MHz spectrometer using a 1.3 mm rotor with recycle delay for 5 s. Spectra were recorded at room temperature and referenced using trimethylsilylpropanoic acid (1.50 ppm relative to TMS) or glycine (33.40 ppm relative to liquid NH_3). The operating frequency was 8.5 kHz. The number of scans varied from 560 to 10000 depending on the compound. Infrared spectra were recorded at room temperature using a Nicolet iS50 FT-IR (Thermo Scientific). The DRIFTS spectra were measured using a Praying Mantis DRIFTS accessory. The spectra of samples are in the 400 – 4000 cm^{-1} range. The spectra are averaging from 128 scans and include atmospheric correction. The spectral resolution was 4 cm^{-1}. High resolution and accurate mass spectra were obtained using a Bruker microTOF-Q spectrometer equipped with an ESI source. Thermogravimetric and differential thermal analyses (simultaneous TG-DTA) were recorded on a Setaram SETSYS 16/18 instrument. Samples for thermogravimetric characterization were placed in alumina crucibles in synthetic air (O_2:N_2 = 40:60) or nitrogen atmosphere (flow rate: $1 \times dm^3 \times h^{-1}$) at heating rate 10 $K \times min^{-1}$. For determination energy of released I_2 different heating rates were applied (5, 10, 20 $K \times min^{-1}$) and studied between 30 and 1000 °C. Preparative separations were performed on a Büchi Sepacore chromatography system. Flash chromatography separations were performed on silica gel grade 60, 40–60 μm mesh. SEM images were collected on a Hitachi S-3400N-II variable-pressure scanning electron microscope. Samples were sputter-coated with 7 nm Au to facilitate viewing by SEM. Energy dispersive X-ray spectra (EDS) were obtained using a EDS Thermo Scientific Ultra Dry system. The skeletal density was tested by the AccuPyc II 1340 helium pycnometer. All gas sorption isotherms were measured on a Micromeritics ASAP 2020. Prior to the measurements, the samples were degassed at 30 °C for 2 h. N_2 sorption measurements were performed at 77 K using a liquid N_2 bath, for CO_2 measurements chilled water-ethylene glycol bath was used for temperature control.

Section 2. Synthesis of prolinkers and PSIFs

Synthesis of octa(3-aminopropyl)silsesquioxane hydrochloride

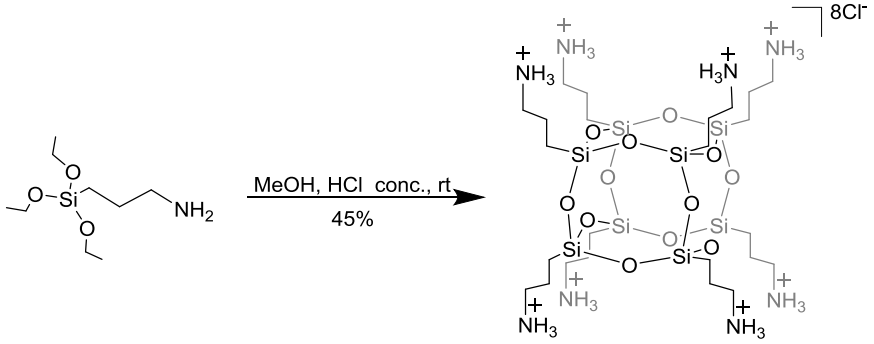

Scheme S1. Synthesis of octa(3-aminopropyl)silsesquioxane hydrochloride.

This compound was synthesized according to previously reported procedure.[1]

^{1}H NMR (500 MHz, DMSO-d$_6$, 300 K): δ 8.23 (s, 24H, N***H***$_3^+$), 2.79 (t, $^{3}J_{HH}$ = 7.9 Hz, 16H, C***H***$_2$NH$_3^+$), 1.74 (m, 16H, SiCH$_2$C***H***$_2$CH$_2$NH$_3^+$), 0.75 (t, $^{3}J_{HH}$ = 8.6 Hz, 16H, SiC***H***$_2$). ^{13}C{^{1}H} NMR (126 MHz, DMSO-d$_6$, 300 K): δ 41.3 (s, SiCH$_2$CH$_2$***C***H$_2$NH$_3^+$), 20.9 (s, SiCH$_2$***C***H$_2$CH$_2$NH$_3^+$), 8.7 (Si***C***H$_2$CH$_2$CH$_2$NH$_3^+$). ^{29}Si{^{1}H} NMR (DMSO-d$_6$, 59.6 MHz, 300 K): δ −66.5. HRMS (ESI+, TOF, MeOH), *m/z*: 881.2887 [M + H − 8HCl]$^+$ (calcd 881.2871), 441.1480 [M + 2H − 8HCl]$^{2+}$ (calcd 441.1472), 294.4340 [M + 3H − 8HCl]$^{3+}$ (calcd 294.4339).

Synthesis of 2',5''-dimethyl-[1,1':4',1''-terphenyl]-4,4''-dicarbaldehyde

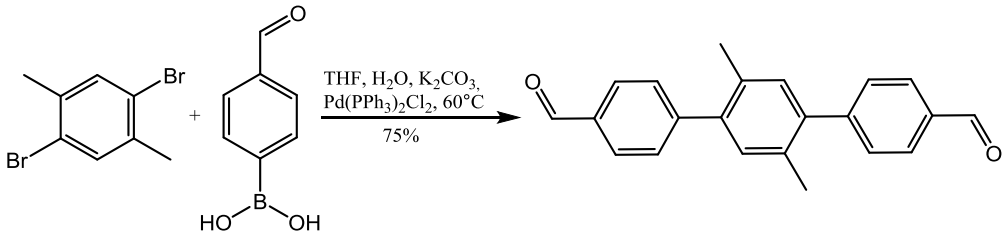

Scheme S2. Synthesis of 2',5'-dimethyl-[1,1':4',1''-terphenyl]-4,4''-dicarbaldehyde.

This compound was synthesized according to a previously reported procedures with some modifications.[3] 1,4-Dibromo-2,5-dimethylbenzene (2.00 g, 7.58 mmol) and 4-formylphenylboronic acid (2.39 g, 15.9 mmol, 2.1 eq) were dissolved in 200 mL of tetrahydrofuran. Aqueous solution of potassium carbonate (8 mL, 2.0 M) was added into the solution under nitrogen atmosphere. The resulting suspension was subjected to three freeze-pump-thaw cycles. After the addition of bis(triphenylphosphine)palladium(II) dichloride (0.266 g, 0.379 mmol, 0.05 eq), the mixture was refluxed for 24 h. After cooling to room temperature, the mixture was extracted twice with dichloromethane (2 × 100 mL). The obtained organic layer was collected and dried with anhydrous sodium sulfate. The crude product was purified by column chromatography on silica gel (hexane/CH_2Cl_2 = 1/1) to give the expected product in a

75% yield (1.80 g, 5.73 mmol) as a white solid. ^{1}H NMR (500 MHz, $CDCl_3$, 300 K): δ 10.08 (s, 2H), 7.96 (d, 4H), 7.55 (d, 4H), 7.18 (s, 2H), 2.30 (s, 6H); $^{13}C\{^{1}H\}$ NMR (126 MHz, $CDCl_3$, 300 K): δ 192.0, 147.9, 140.3, 135.2, 132.8, 131.9, 130.0, 129.8, 20.0.

Synthesis of 1,3,5-benzenetricarbaldehyde

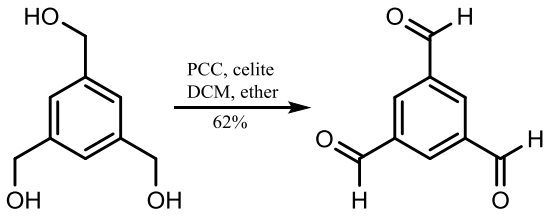

Scheme S3. Synthesis of 1,3,5-benzenetricarbaldehyde.

This compound was synthesized according to a previously reported procedure,[4] starting from 0.99 g (5.9 mmol) of 1,3,5-tris(hydroxymethyl)benzene. Yield 0.602 g (62%). ^{1}H NMR (500 MHz, $CDCl_3$, 300 K): δ 10.21 (s, 3H, CHO), 8.67 (s, 3H, Ar2,4,6-H). $^{13}C\{^{1}H\}$ NMR (126 MHz, $CDCl_3$, 300 K): δ 191.0 (CHO), 137.9 ($Ar_{1,3,5}$-*C*), 135.6 ($Ar_{2,4,6}$-*C*).

Synthesis of 2,4,6-trihydroxybenzene-1,3,5-tricarbaldehyde

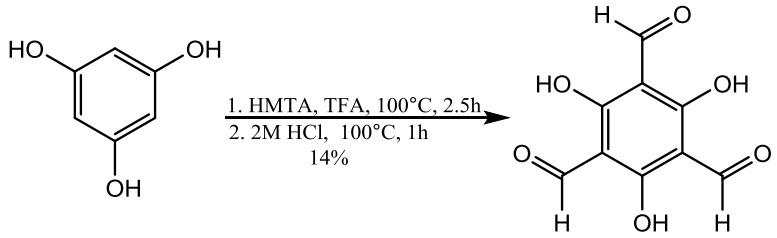

Scheme S4. Synthesis of 2,4,6-trihydroxybenzene-1,3,5-tricarbaldehyde.

This compound was synthesized according to a previously reported procedure,[4] starting from 6.0 g (49 mmol) of 1,3,5-benzenetriol. Yield 1.48 g (14%). ^{1}H NMR (500 MHz, $CDCl_3$, 300 K): δ 14.10 (s, 3H, −O*H*), 10.14 (s, 3H, −C*H*O), $^{13}C\{^{1}H\}$ NMR (126 MHz, $CDCl_3$, 300 K): δ 192.2 , 173.7, 103.0.

Synthesis of 1,3,5-tris(4-formylphenyl)benzene

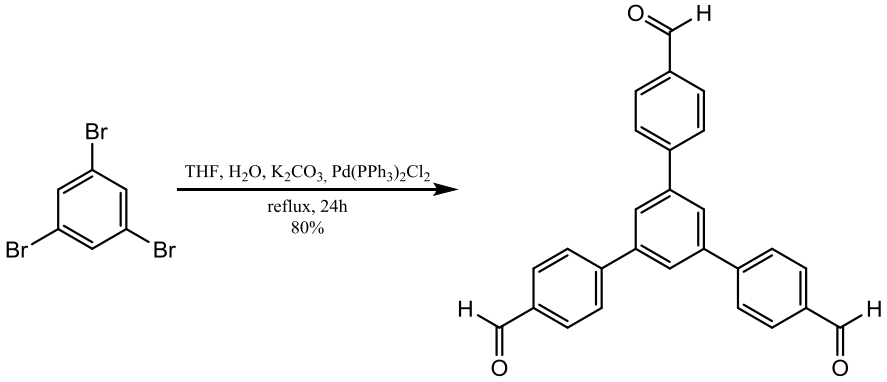

Scheme S5. Synthesis of 1,3,5-tris(4-formylphenyl)benzene.

This compound was synthesized according to a previously reported procedures with some modifications.[7] 1,3,5-tribromobenzene (1.00 g, 3.18 mmol) and 4-formylphenylboronic acid (1.45 g, 9.69 mmol, 3.05 eq) were dissolved in 100 mL of tetrahydrofuran. Aqueous solution of potassium carbonate (5.0 mL, 2.0 M) was added to the solution under nitrogen atmosphere. The resulting suspension was subjected to the freeze-pump-thaw cycles. After the addition of bis(triphenylphosphine)palladium(II) dichloride (0.301 g, 0.429 mmol, 0.135 eq), the mixture was refluxed for 24 h. After cooling to room temperature, the mixture was extracted twice with dichloromethane (2 × 100 mL). The obtained organic layer was collected and dried with anhydrous sodium sulfate. After that, the solvent was removed under reduced pressure. The crude product was then dissolved in DCM and run through a plug of silica. The solvent was next evaporated and the resulting solid was recrystallized from MeCN. Yield 80% (1.00 g, 2.56 mmol). ^{1}H NMR (500 MHz, $CDCl_3$, 300 K): δ 10.10 (s, 3H), 8.02 (d, 6H), 7.91 (s, 3H), 7.86 (d, 6H), $^{13}C\{^{1}H\}$ NMR (126 MHz, $CDCl_3$, 300 K): δ 191.8, 146.4, 141.7, 135.9, 130.5, 128.1, 126.6.

Synthesis of PSIF-1

A 20 mL pyrex vial was charged with octa(3-aminopropyl)silsesquioxane hydrochloride (0.200 g, 0.170 mmol), 1,4-phthalaldehyde (0.091 g, 0.682 mmol, 4 eq), dimethyl sulfoxide (10 mL) and triethylamine (0.190 mL, 1.364 mmol), the mixture was sonicated for 2 minutes. The vial was placed in an oven at 60 °C for 1 h. After the reaction a white sol was formed.

Synthesis of PSIF-2

A 20 mL pyrex vial was charged with octa(3-aminopropyl)silsesquioxane hydrochloride (0.200 g, 0.170 mmol), 2',5'-dimethyl-[1,1':4',1"-terphenyl]-4,4"-dicarbaldehyde (0.214 g, 0.682 mmol, 4 eq), dimethyl sulfoxide (10 mL) and triethylamine (0.190 mL, 1.364 mmol), the mixture was sonicated for 2 minutes. The vial was placed in an oven at 60 °C for 12 h. After the reaction a white sol was formed.

Synthesis of PSIF-3

A 20 mL pyrex vial was charged with octa(3-aminopropyl)silsesquioxane hydrochloride (0.200 g, 0.170 mmol), 1,3,5-benzenetricarbaldehyde (0.074 g, 0.454 mmol, 2.67 eq), dimethyl sulfoxide (10 mL) and triethylamine (0.190 mL, 1.364 mmol), the mixture was sonicated for 2 minutes. The vial was placed in an oven at 60 °C for 2 h. After the reaction white a sol was formed.

Synthesis of PSIF-4

A 20 mL pyrex vial was charged with octa(3-aminopropyl)silsesquioxane hydrochloride (0.200 g, 0.170 mmol), 2,4,6-trihydroxybenzene-1,3,5-tricarbaldehyde (0.074 g, 0.454 mmol, 2.67 eq), dimethyl sulfoxide (10 mL) and triethylamine (0.190 mL, 1.364 mmol), the mixture was sonicated for 2 minutes. The vial was placed in an oven at 60 °C for 12 h. After the reaction a white sol was formed.

Synthesis of PSIF-5

A 20 mL pyrex vial was charged with octa(3-aminopropyl)silsesquioxane hydrochloride (0.200 g, 0.170 mmol), 1,3,5- tris(4-formylphenyl)benzene (0.177 g, 0.454 mmol, 2.67 eq), dimethyl sulfoxide (10 mL) and triethylamine (0.190 mL, 1.364 mmol), the mixture was sonicated for 2 minutes. The vial was placed in an oven at 60 °C for 12 h. After the reaction a white sol was formed.

Section 3. Structural characterization of PSIFs

1. Solubility tests

Typically 1–5 mg of activated PSIF was placed in a 25 ml round bottom flask containing 5 ml of tested solvent (benzene, chlorobenzene, chloroform, cyclohexane, dimethyl sulfoxide, ethanol, hexane, mesitylene, tetrahydrofuran and toluene). The suspension was refluxed for 24 h. After cooling to room temperature, suspensions were separated by centrifugation. Next, the supernatant was evaporated to dryness. All samples did not show any measureable solubility in tested solvents.

2. Photographs.

a)  b) 

Figure S1. Photographic images of **PSIF-1** gel a) after reaction; b) after Soxhlet extraction with ethanol.

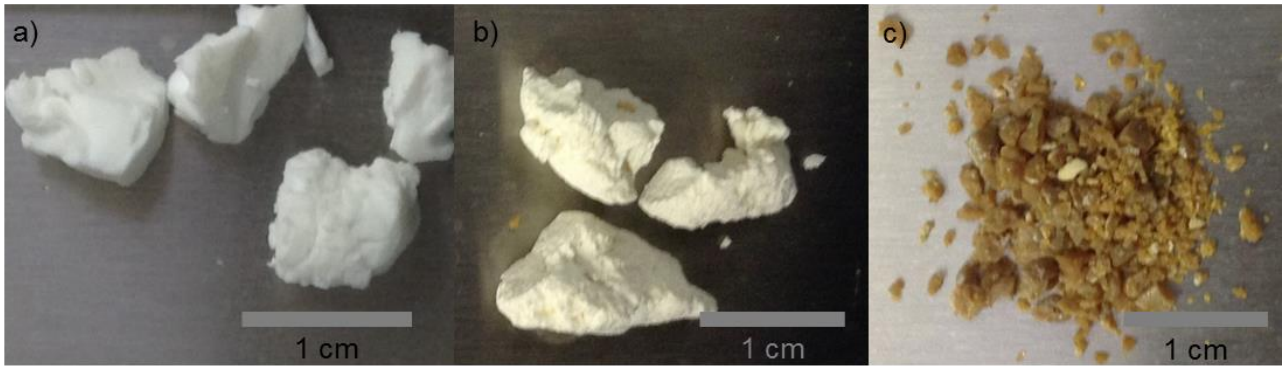

Figure S2. Photography of activated **PSIF-1**: a) supercritical carbon dioxide dried (**PSIF-1a**), b) freeze-dried (**PSIF-1b**), c) thermally activated (**PSIF-1c**).

3. NMR spectral characterization of PSIFs in solution and solid state

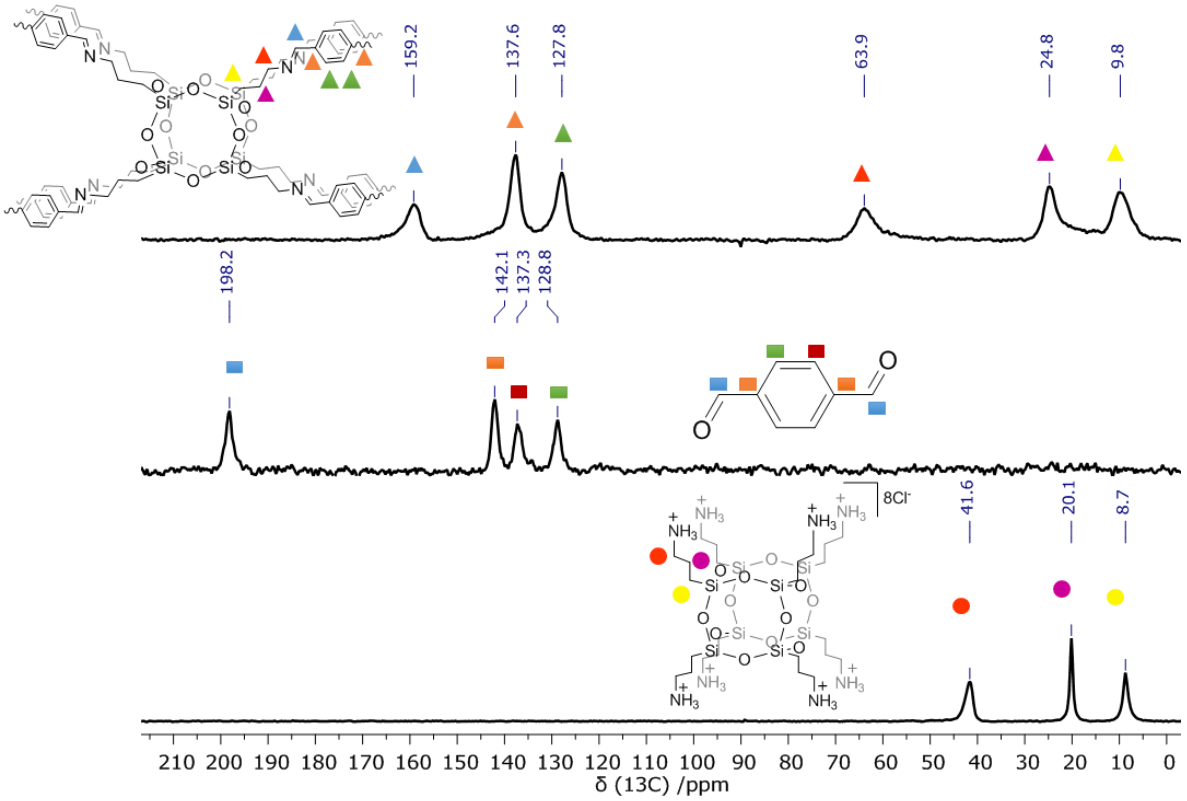

Figure S3. ^{13}C CP-MAS NMR spectra of OAS-POSS-NH_3Cl (bottom), 1,4-phthalaldehyde (middle), and **PSIF-1a** (top).

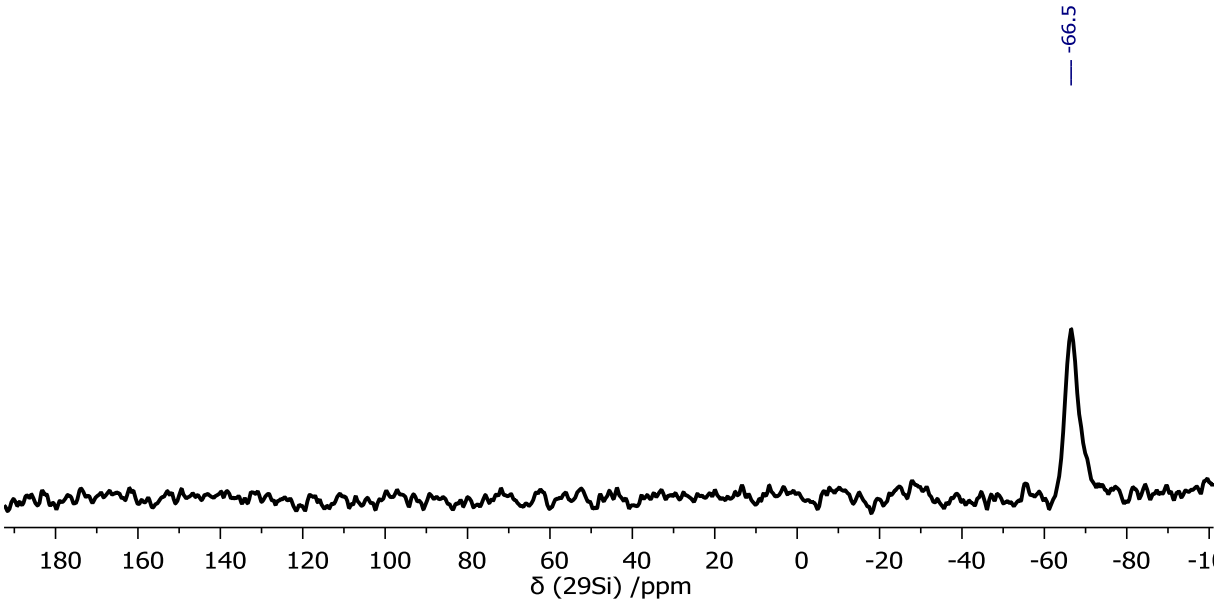

Figure S4. ^{29}Si CP-MAS NMR spectrum of **PSIF-1a**.

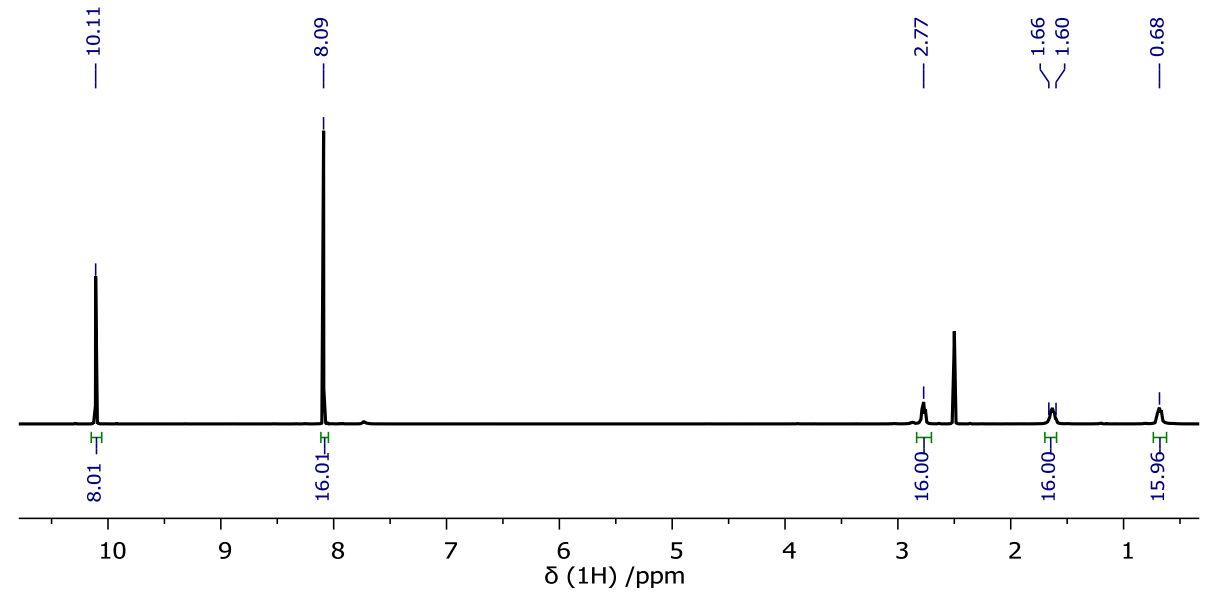

Figure S5. ^{1}H NMR spectrum of **PSIF-1a** in DMSO-d_6/D_2SO_4 mixture.

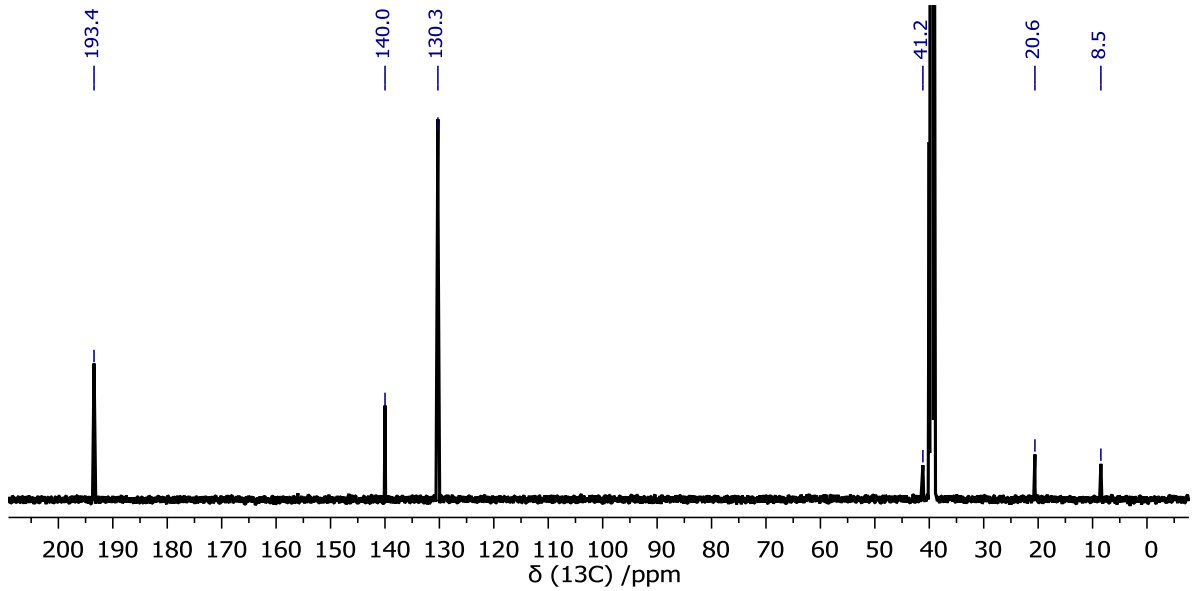

Figure S6. ^{13}C NMR spectrum of **PSIF-1a** in DMSO-d_6/D_2SO_4 mixture.

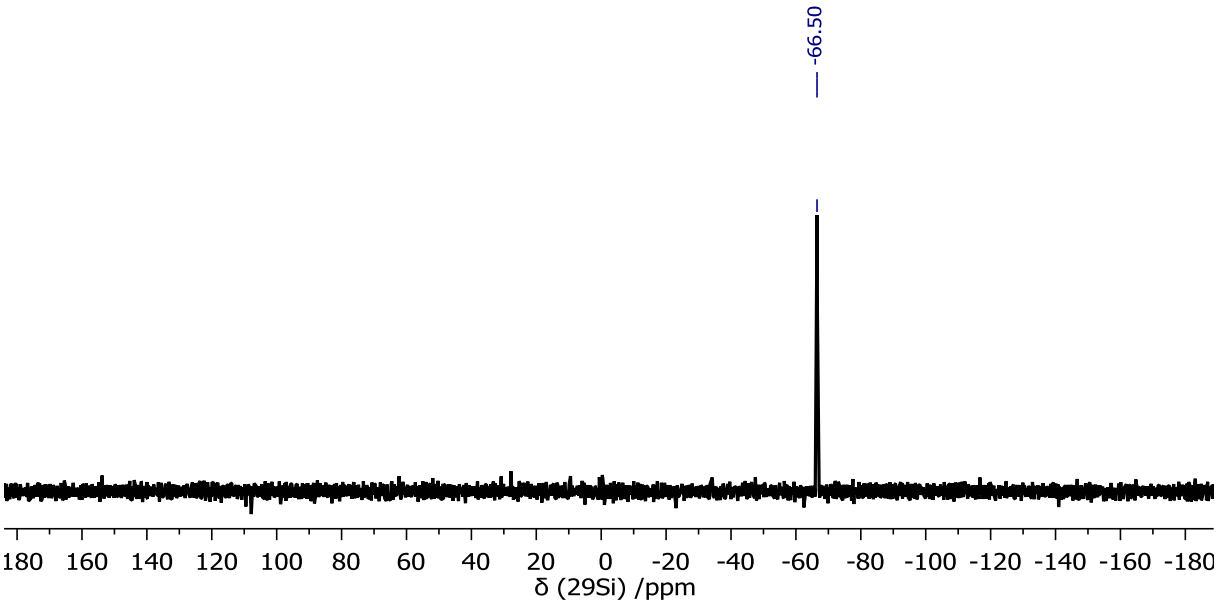

Figure S7. ^{29}Si NMR spectrum of **PSIF-1a** in DMSO-d_6/D_2SO_4 mixture.

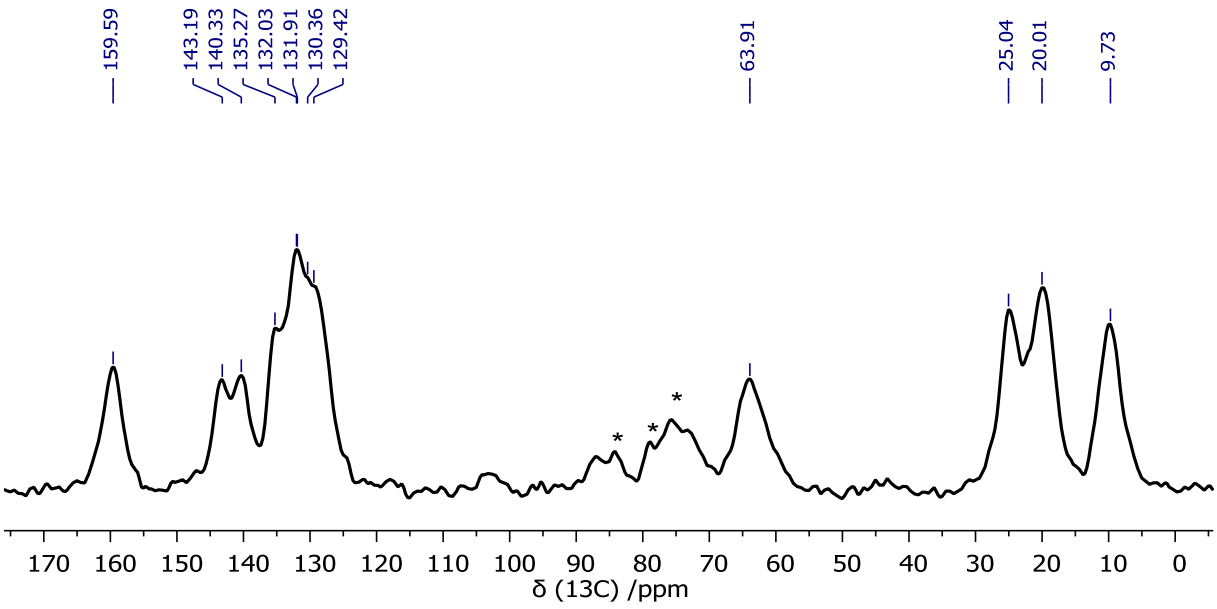

Figure S8. ^{13}C CP-MAS NMR spectrum of **PSIF-2a**. Asterisks designate spinning side bands.

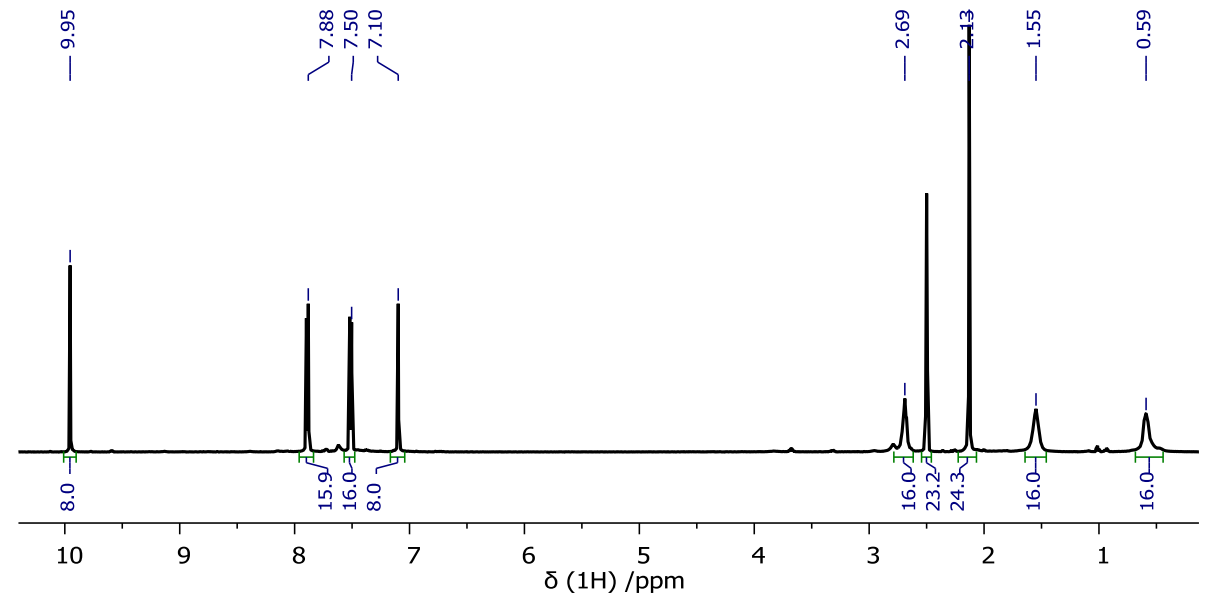

Figure S9. ^{1}H NMR spectrum of **PSIF-2a** in DMSO-d_6/D_2SO_4 mixture.

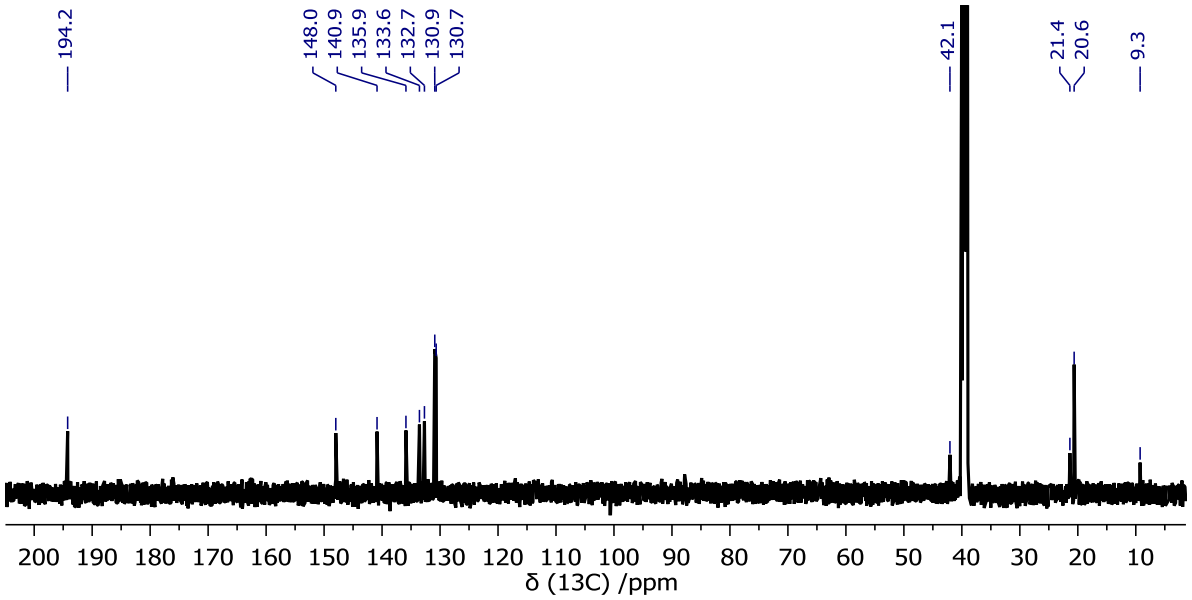

Figure S10. ^{13}C NMR spectrum of **PSIF-2a** in DMSO-d_6/D_2SO_4 mixture.

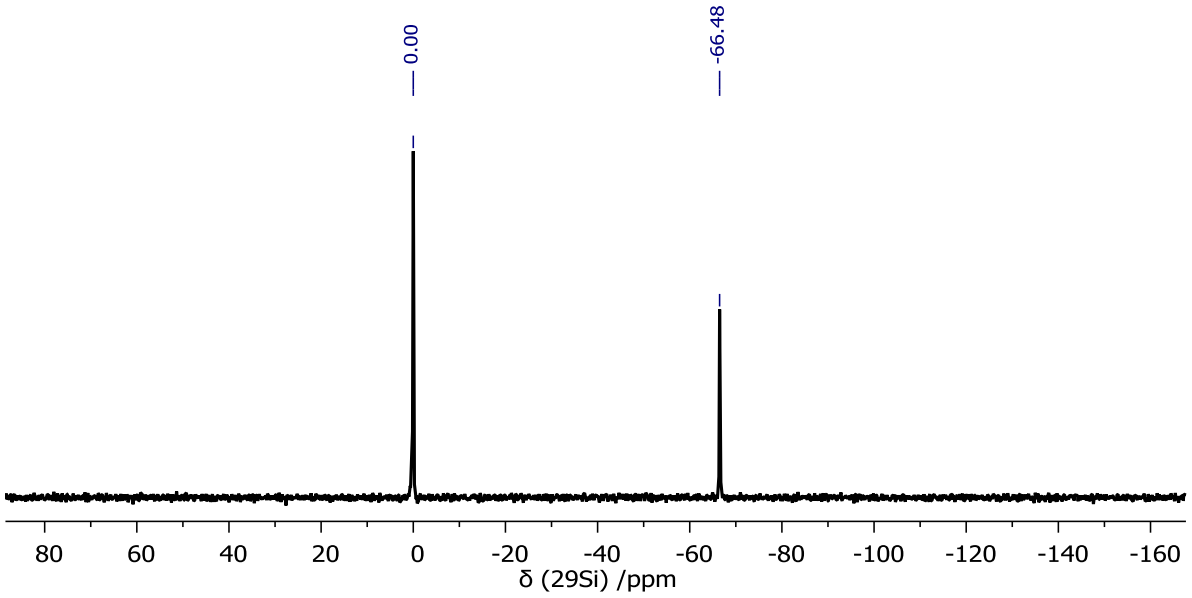

Figure S11. ^{29}Si NMR spectrum of **PSIF-2a** in DMSO-d_6/D_2SO_4 mixture.

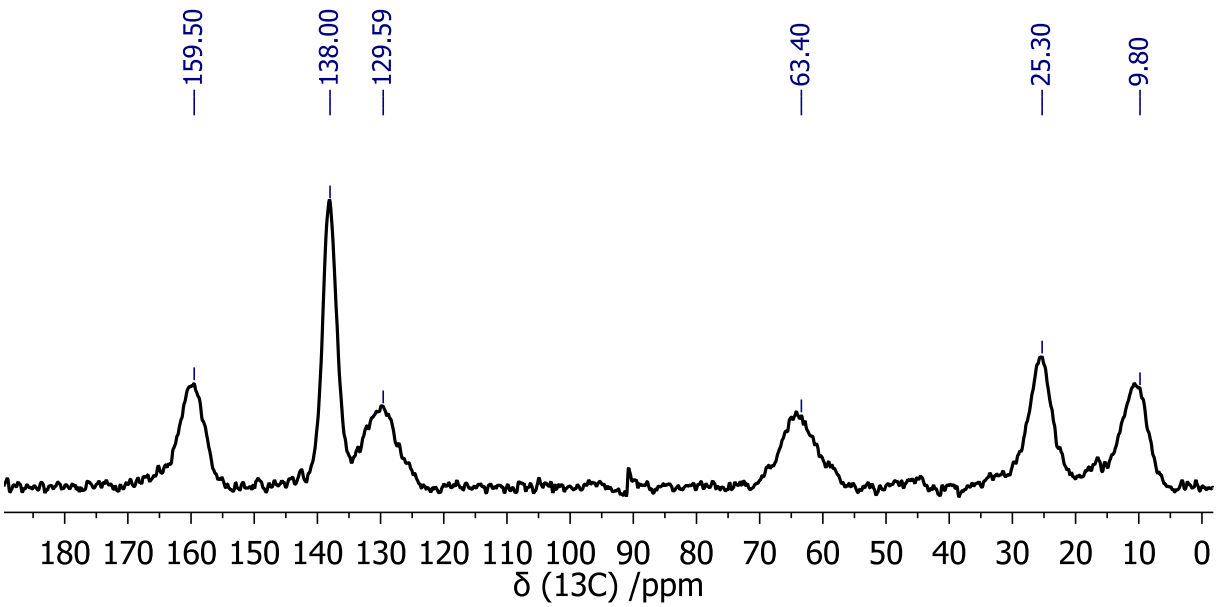

Figure S12. ^{13}C CP-MAS NMR spectrum of **PSIF-3a**.

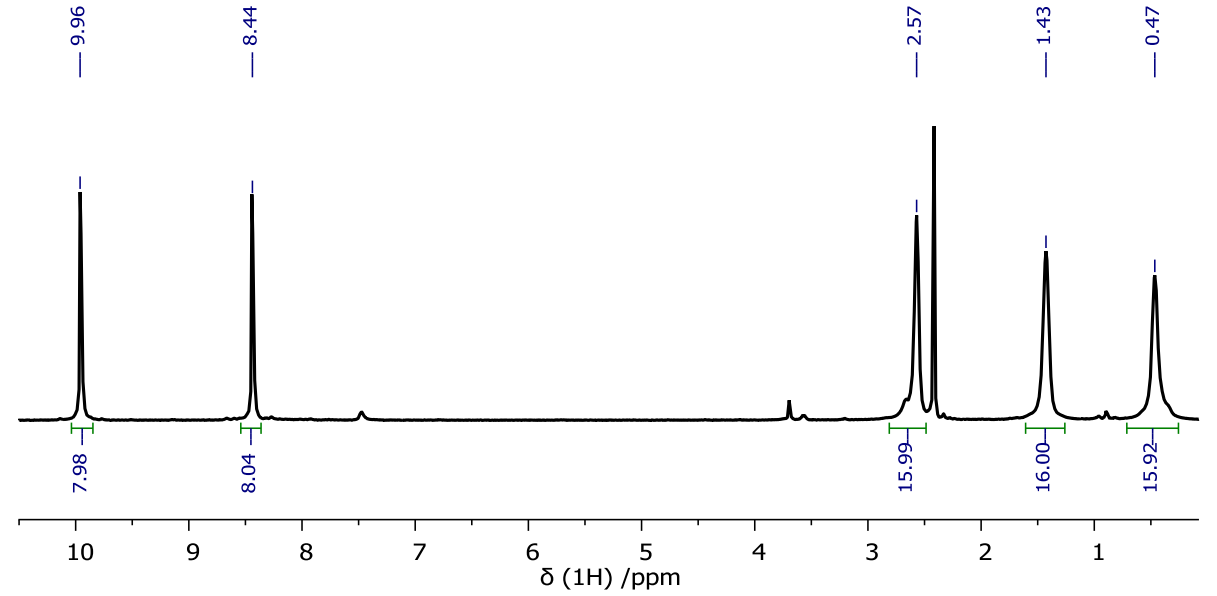

Figure S13. ^{1}H NMR spectrum of **PSIF-3a** in DMSO-d_6/D_2SO_4 mixture.

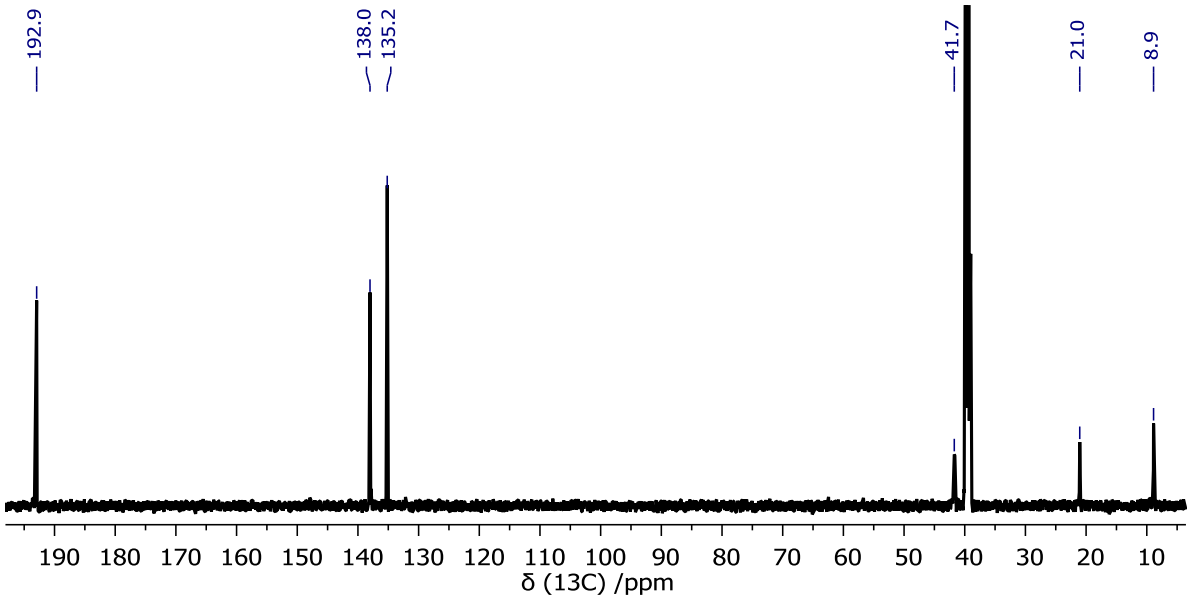

Figure S14. ^{13}C NMR spectrum of **PSIF-3a** in DMSO-d_6/D_2SO_4 mixture.

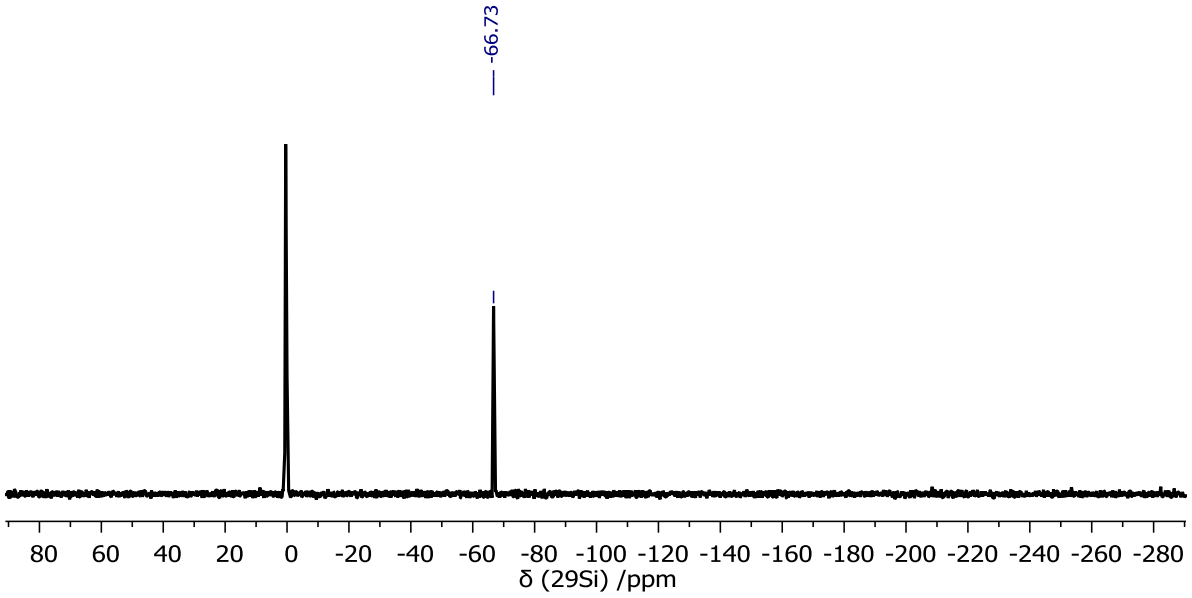

Figure S15. ^{29}Si NMR spectrum of **PSIF-3a** in DMSO-d_6/D_2SO_4 mixture.

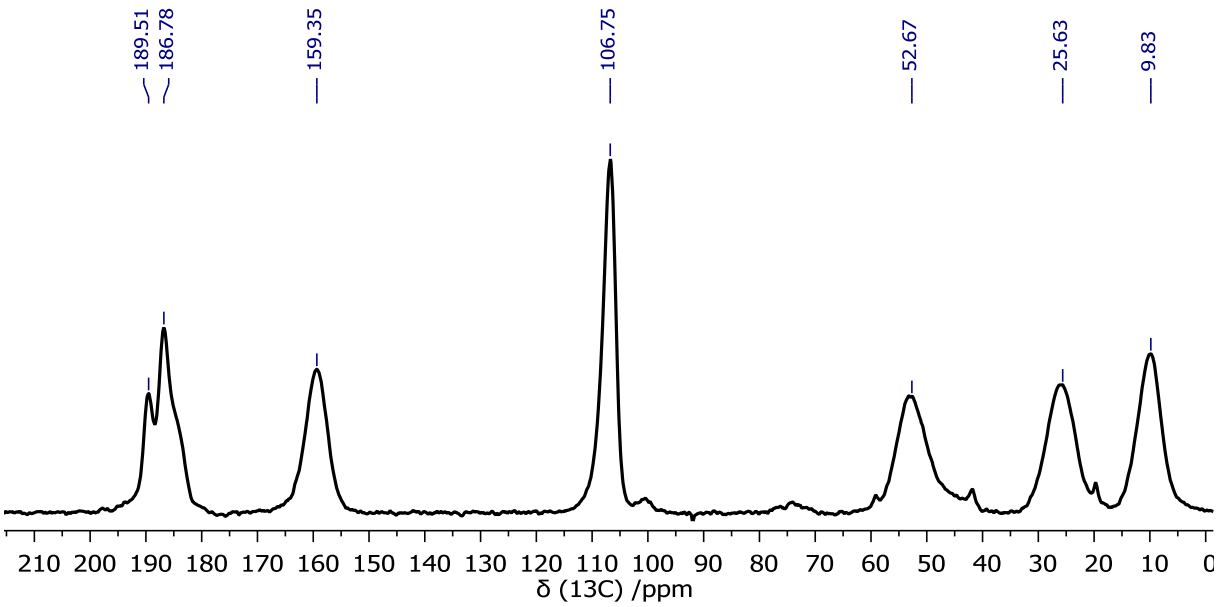

Figure S16. ^{13}C CP-MAS NMR spectrum of **PSIF-4a**.

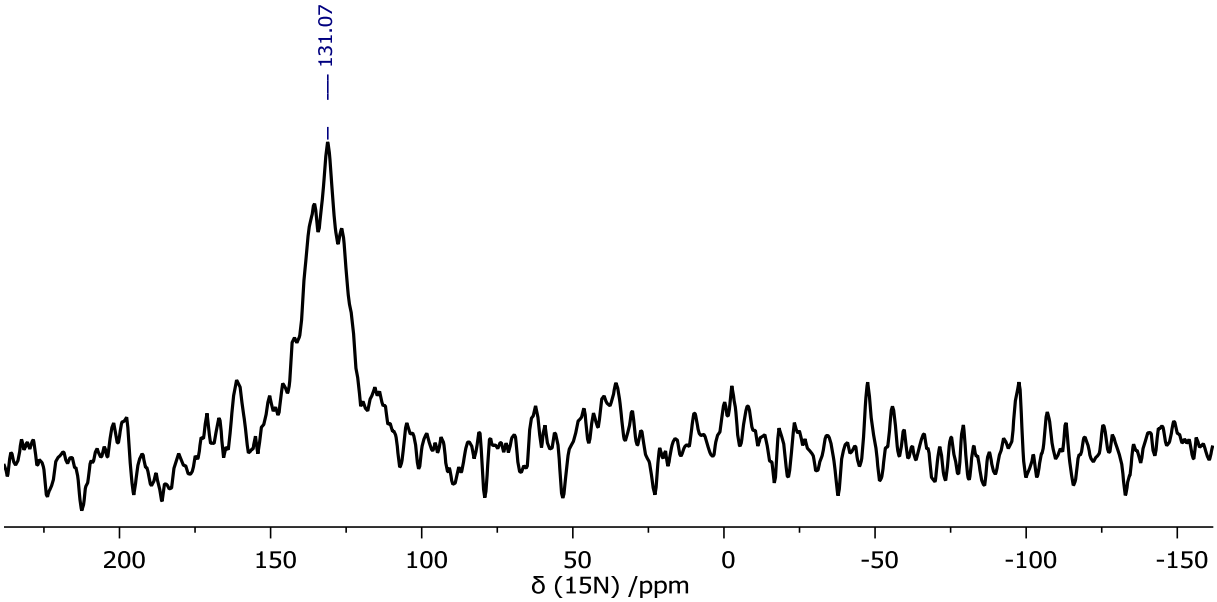

Figure S17. ^{15}N CP-MAS NMR spectrum of **PSIF-4a**.

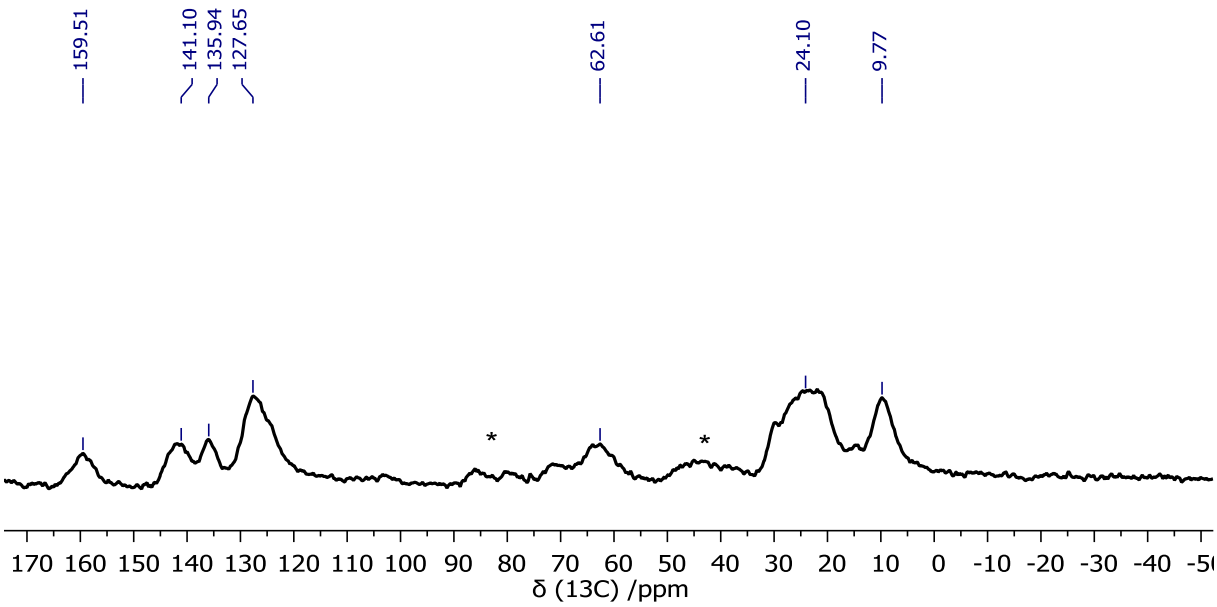

Figure S18. ^{13}C CP-MAS NMR spectrum of **PSIF-5a**. Asterisks designate spinning side bands.

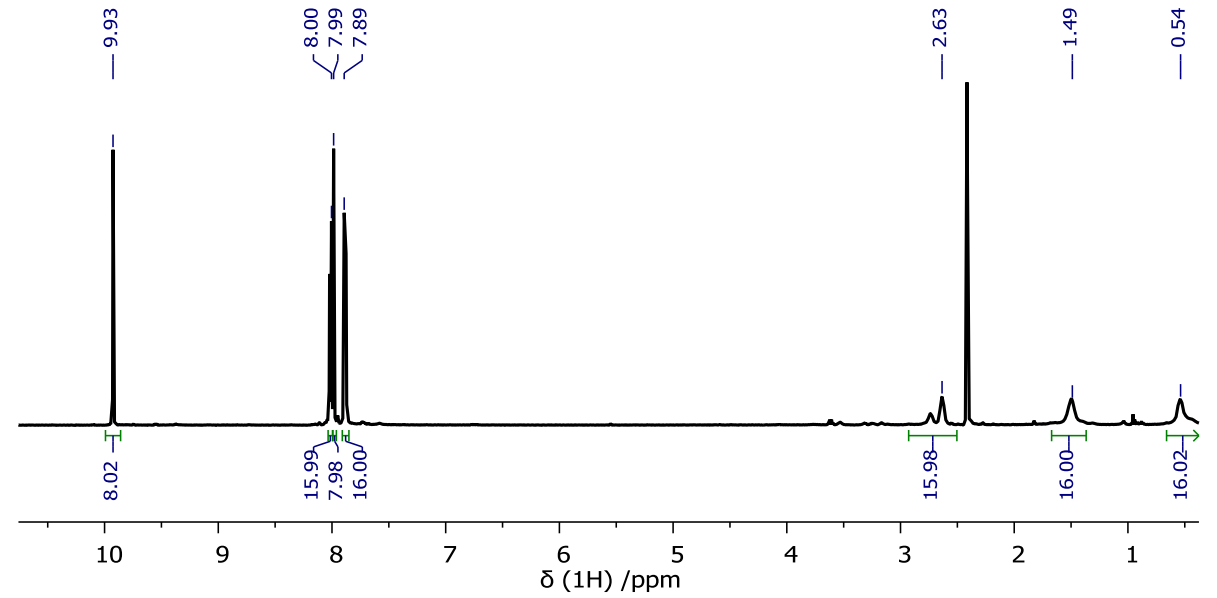

Figure S19. ^{1}H NMR spectrum of **PSIF-5a** in DMSO-d_6/D_2SO_4 mixture.

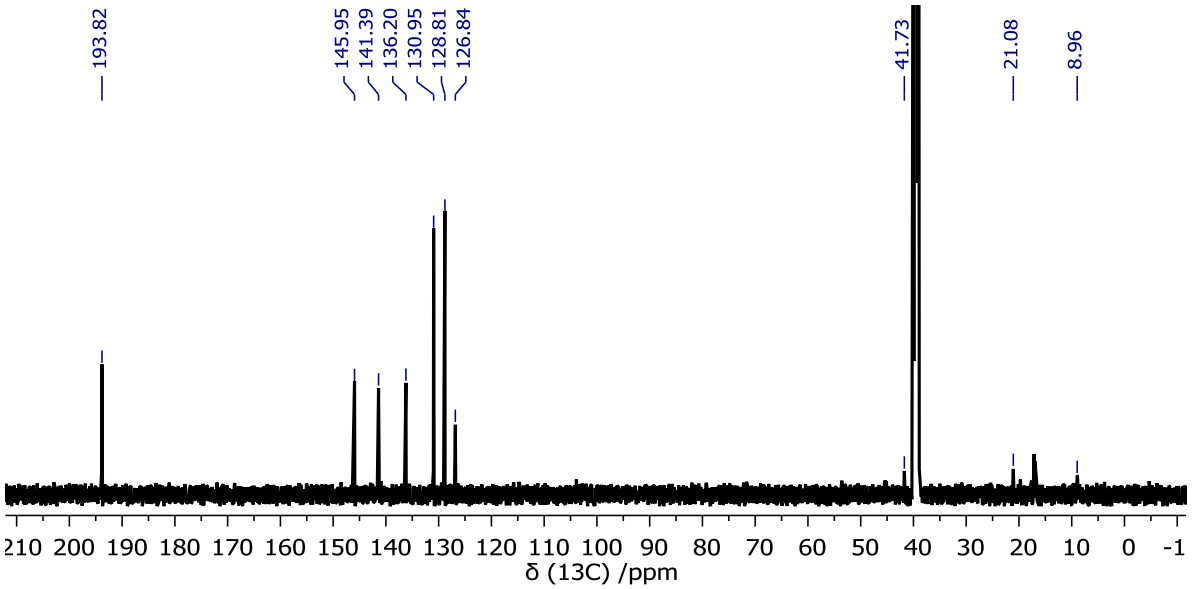

Figure S20. ^{13}C NMR spectrum of **PSIF-5a** in DMSO-d_6/D_2SO_4 mixture.

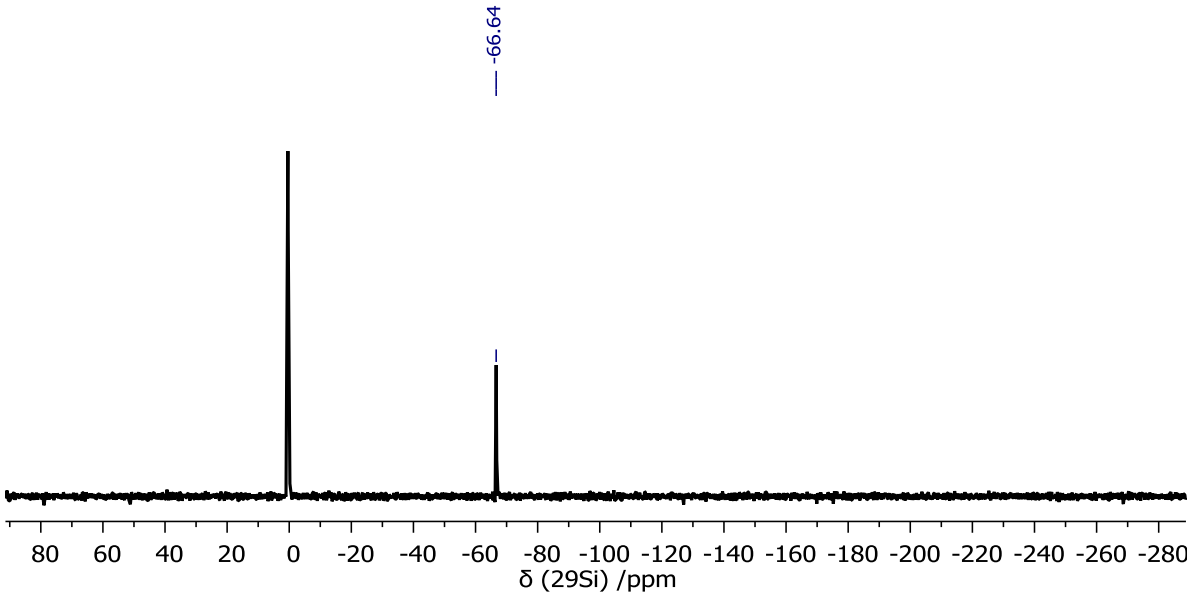

Figure S21. ^{29}Si NMR spectrum of **PSIF-5a** in DMSO-d_6/D_2SO_4 mixture.

4. SEM images and EDS analysis

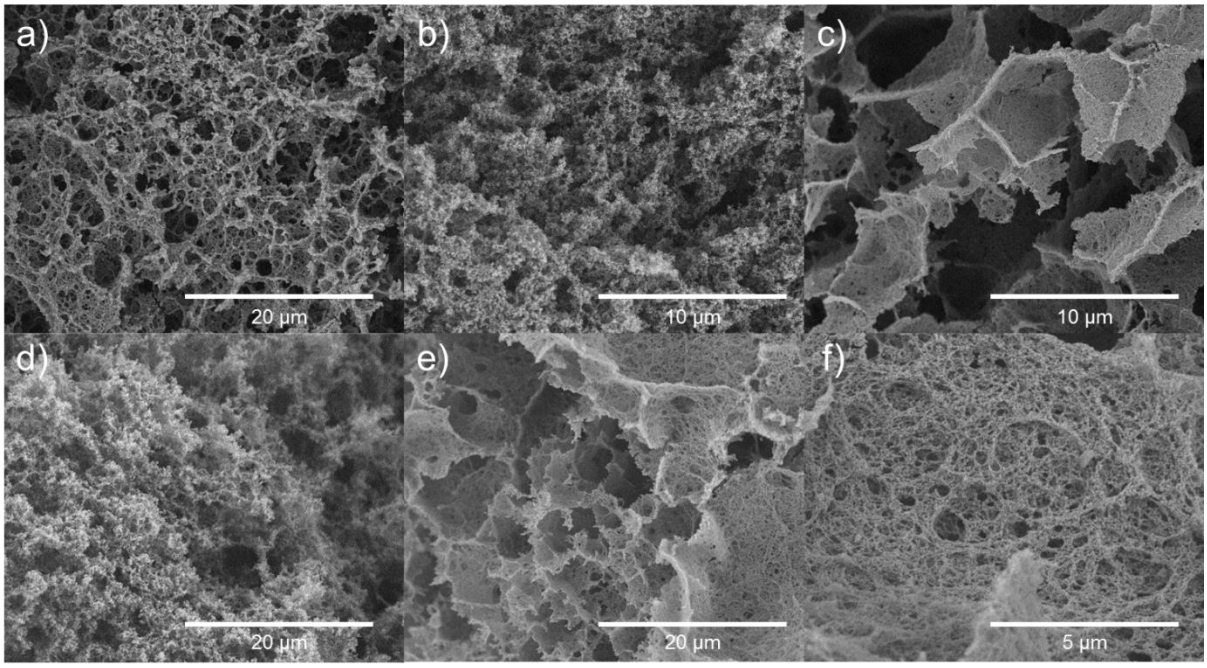

Figure S22. SEM images of the PSIFs: (a) **PSIF-1a**; (b) **PSIF-2a**; (c) **PSIF-3a**; (d) **PSIF-4a**; (e, f) **PSIF-5a**.

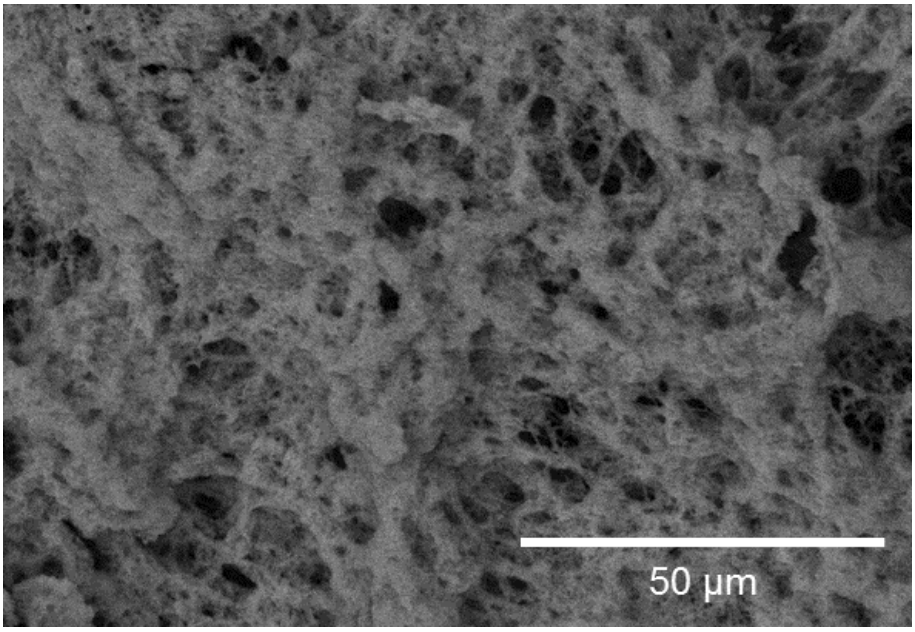

Figure S23. SEM images of the **I_2@PSIF-1a**.

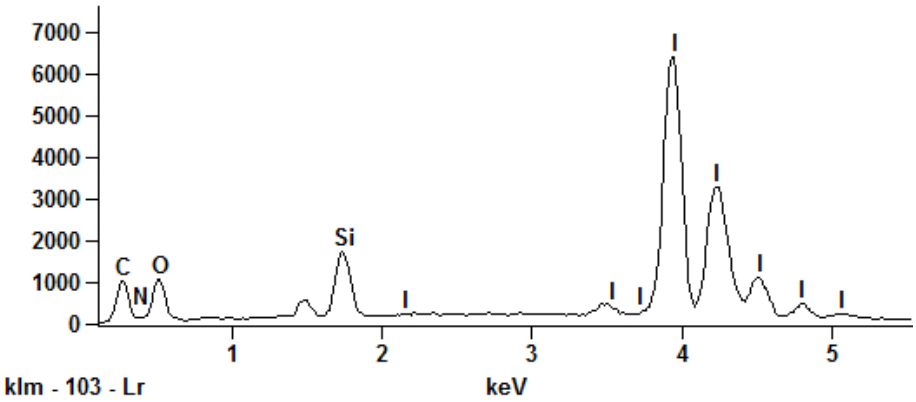

Figure S24. EDS spectrum of the **I_2@PSIF-1a**.

5. Adsorption of N_2 and BET surface area calculations

The Brunauer-Emmett-Teller (BET) method was utilized to calculate the specific surface areas. By using the non-local density functional theory (DFT) model, the pore size distribution (PSD) curve was derived from the sorption data.

Table S1. BET parameters for **PSIF-1a**.

Parameter	*Value*
C	48.5
Q_m [cm^3/g STP]	73.4
BET [m^2/g]	320

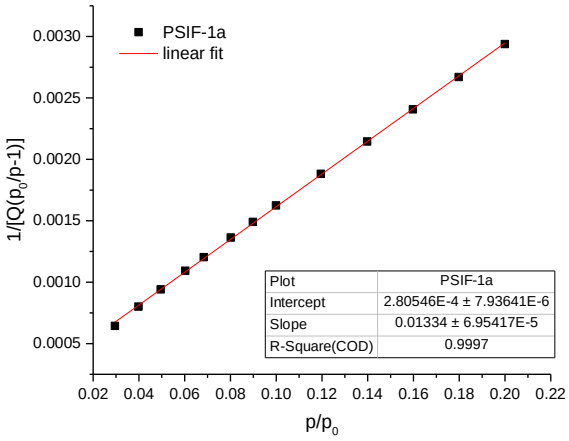

Figure S25. BET plot and fitting parameters for **PSIF-1a**.

Table S2. BET parameters for **PSIF-2a**.

Parameter	*Value*
C	58.3
Q_m [cm^3/g STP]	60.2
BET [m^2/g]	262

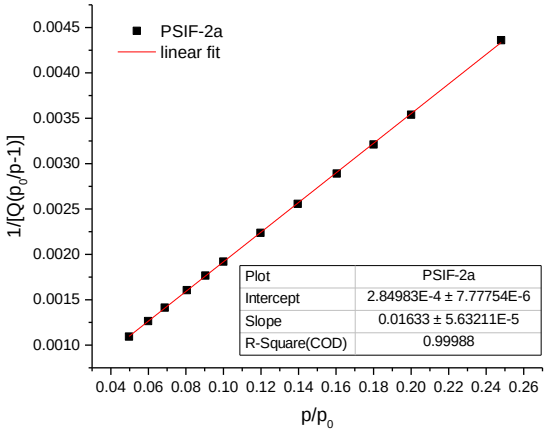

Figure S26. BET plot and fitting parameters for **PSIF-2a**.

Table S3. BET parameters for **PSIF-3a**.

Parameter	*Value*
C	70.0
Q_m [cm^3/g STP]	108.7
BET [m^2/g]	473

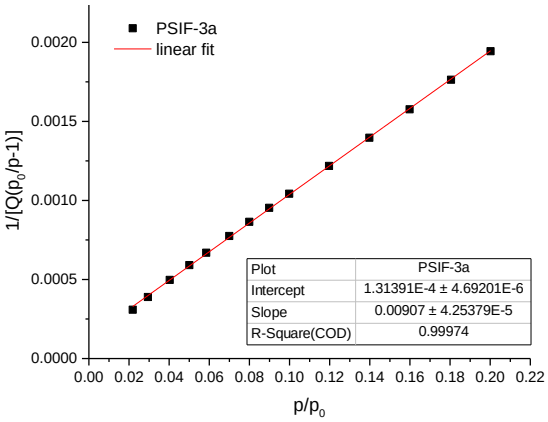

Figure S27. BET plot and fitting parameters for **PSIF-3a**.

Table S4. BET parameters for **PSIF-4a**.

Parameter	*Value*
C	126.9
Q_m [cm^3/g STP]	48.2
BET [m^2/g]	209.6

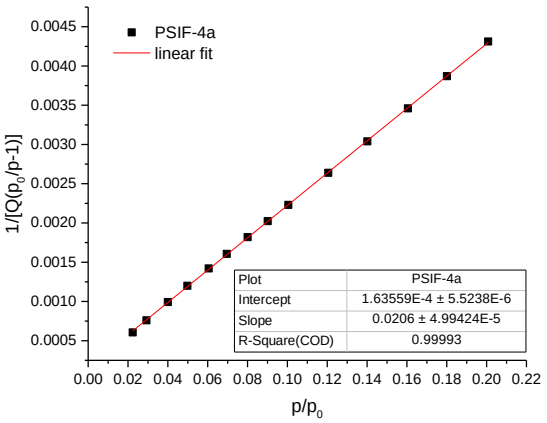

Figure S28. BET plot and fitting parameters for **PSIF-4a**.

Table S5. BET parameters for **PSIF-5a**.

Parameter	*Value*
C	120.7
Q_m [cm^3/g STP]	131.8
BET [m^2/g]	574

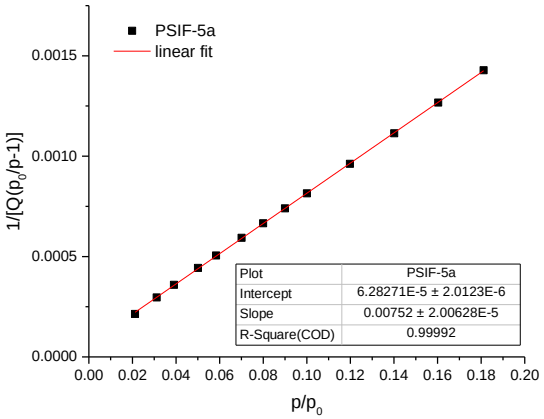

Figure S29. BET plot and fitting parameters for **PSIF-5a**.

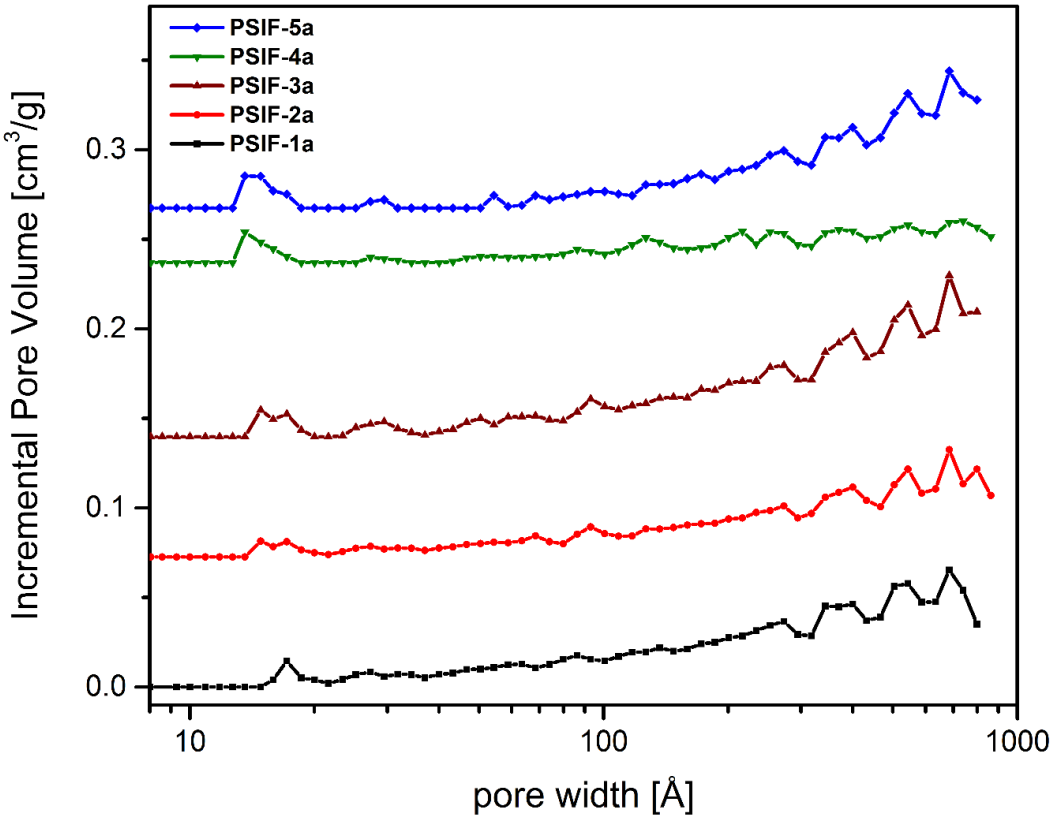

Figure S30. DFT incremental pore volume distribution for **PSIFs**.

6. Adsorption of CO_2 and isosteric heats of CO_2 adsorption (Q_{st})

The CO_2 adsorption experiments were carried out at 263, 273, 283 and 293 K up to 1.0 bar. The isosteric heats of adsorption (Q_{st}) were calculated by fitting the CO_2 adsorption isotherms using the single-site (**PSIF-1a**) or dual-site (**PSIF-2a**–**5a**) Langmuir model and Clausius – Clapeyron equation.[8] The CO_2 isotherms for **PSIF** samples show Langmuir type behavior. Isotherms were measured for these samples at four temperatures (263, 273, 283 and 293 K) and they were subsequently fit with the dual-site Langmuir model, according to eq 1:[8]

$$q \equiv q_A + q_B = \frac{q_{sat,A} \times b_A \times p}{1 + b_A \times p} + \frac{q_{sat,B} \times b_B \times p}{1 + b_B \times p} \quad (1)$$

where q is the total gravimetric uptake of CO_2 (mmol/g) at pressure p; $q_{sat,i}$ and b_i are saturation loading and Langmuir affinity parameter for site i, respectively.

The temperature dependences of the two Langmuir constants b_A and b_B are described by eqs 2 and 3:

$$b_A = b_{A0} \times exp\left(\frac{E_A}{RT}\right) \quad (2)$$

$$b_B = b_{B0} \times exp\left(\frac{E_B}{RT}\right) \quad (3)$$

where E_A, E_B are heats of adsorption for site A and B, b_{A0} and b_{B0} are the pre-exponential parameters and R is the gas constant.

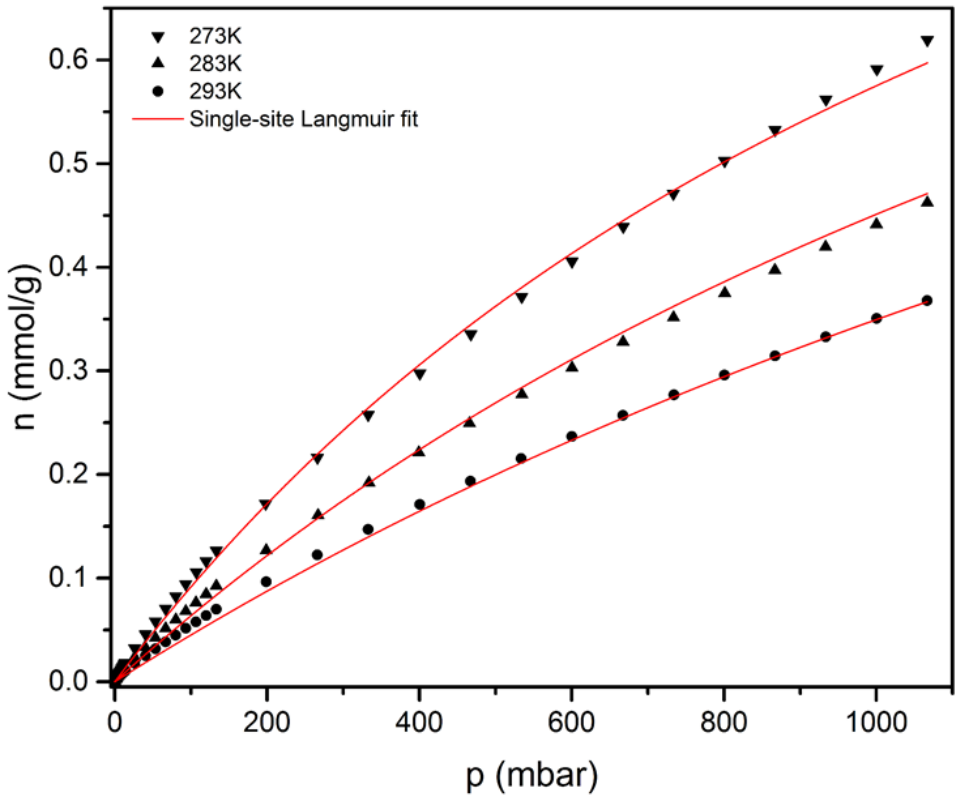

Figure S31. CO_2 isotherms for **PSIF-1a**.

Table S6. Single-site Langmuir parameters for adsorption of CO_2 in **PSIF-1a**. These parameters were determined by fitting adsorption isotherms for temperatures ranging from 273 K to 293 K.

Parameter	*Value*
$q_{sat,A}$	1.39 mol/kg
b_{A0}	1.34×10^{-8} Pa^{-1}
E_A	24.7 kJ/mol
$q_{sat,B} = 0$; $b_{B0} = 0$; $E_B = 0$	

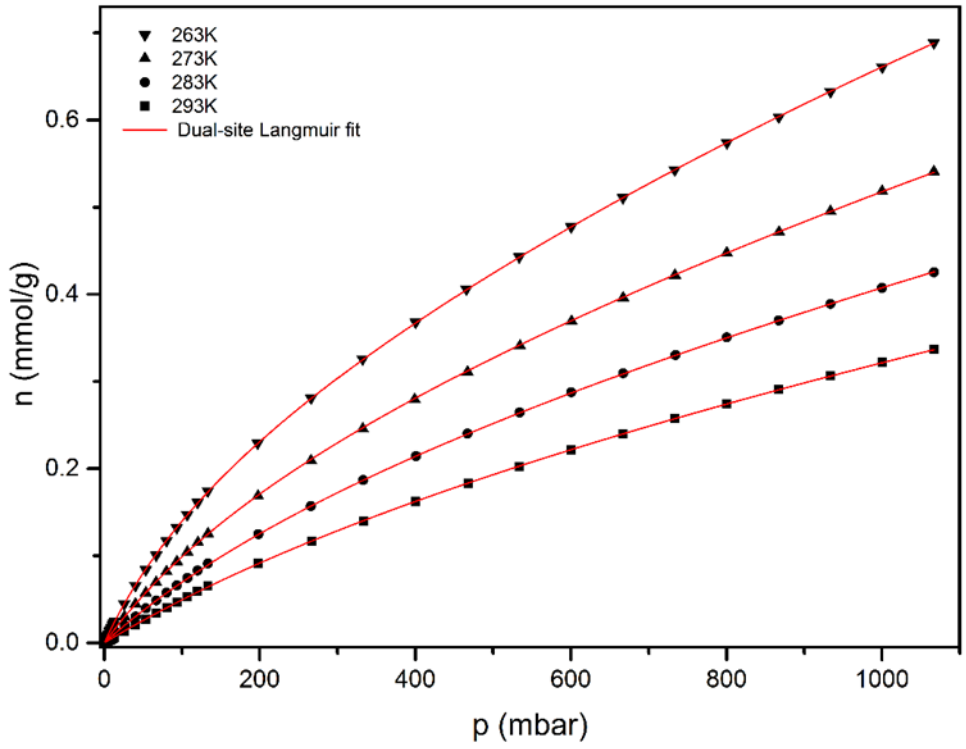

Figure S32. CO_2 isotherms for **PSIF-2a**.

Table S7. Dual-site Langmuir parameters for adsorption of CO_2 in **PSIF-2a**. These parameters were determined by fitting adsorption isotherms for temperatures ranging from 263 K to 293 K.

Parameter	*Value*
$q_{sat,A}$	0.213 mol/kg
$q_{sat,B}$	2.62 mol/kg
b_{A0}	7.49×10^{-9} Pa^{-1}
E_A	29.8 kJ/mol
b_{B0}	8.81×10^{-9} Pa^{-1}
E_B	22.2 kJ/mol

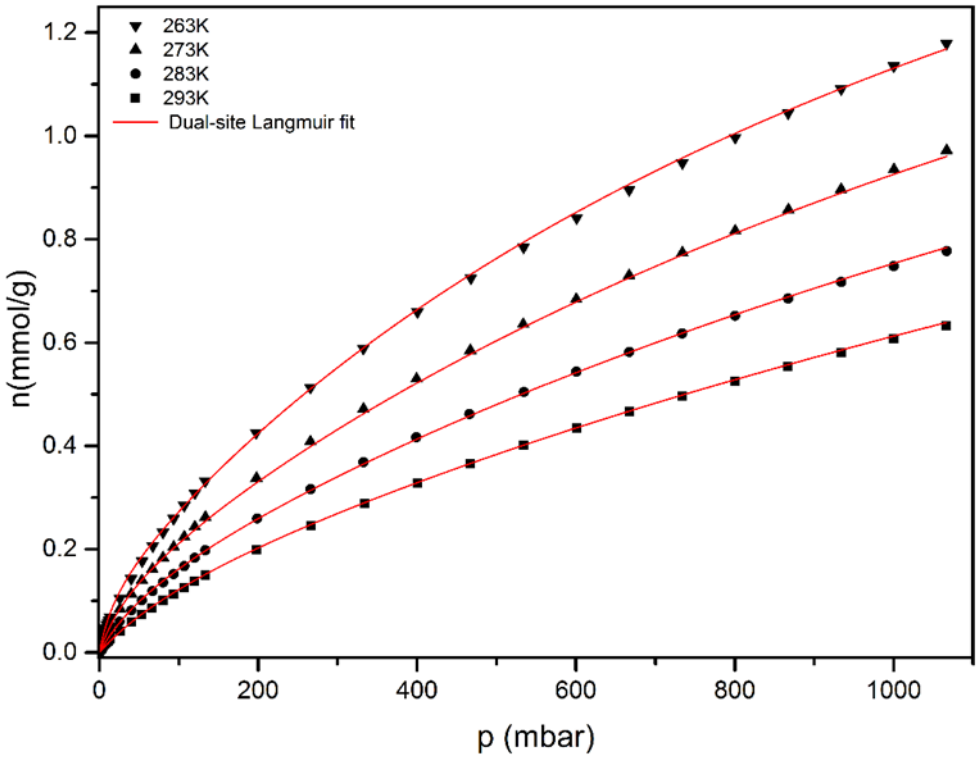

Figure S33. CO_2 isotherms for **PSIF-3a**.

Table S8. Dual-site Langmuir parameters for adsorption of CO_2 in **PSIF-3a**. These parameters were determined by fitting adsorption isotherms for temperatures ranging from 263 K to 293 K.

Parameter	*Value*
$q_{sat,A}$	0.13 mol/kg
$q_{sat,B}$	2.36 mol/kg
b_{A0}	1.78×10^{-9} Pa^{-1}
E_A	37.5 kJ/mol
b_{B0}	3.33×10^{-8} Pa^{-1}
E_B	21.9 kJ/mol

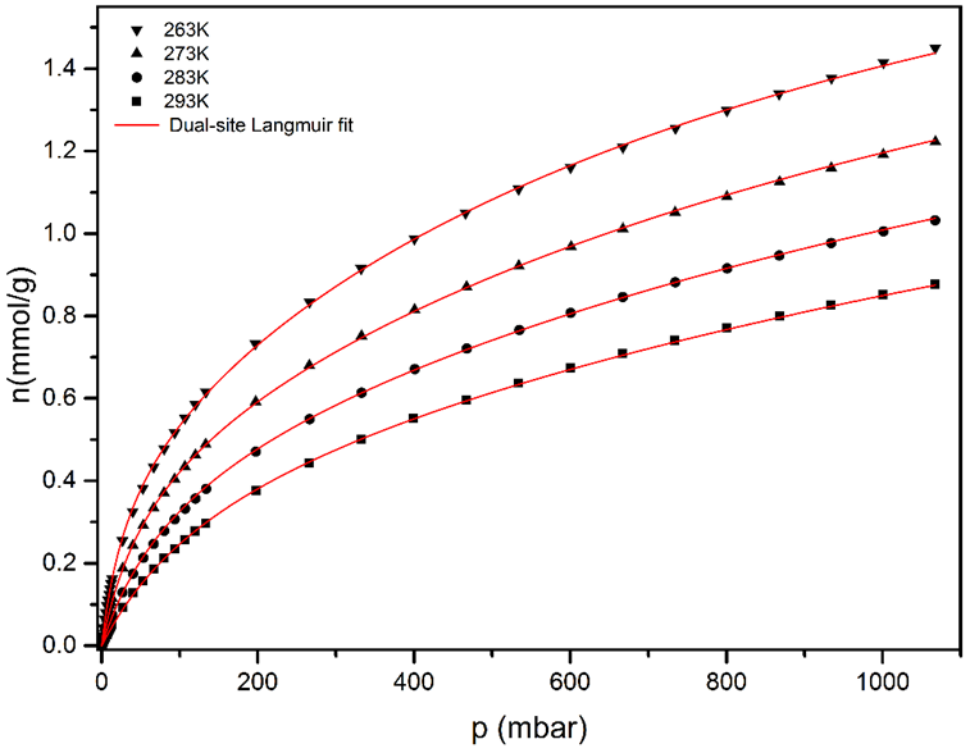

Figure S34. CO_2 isotherms for **PSIF-4a**.

Table S9. Dual-site Langmuir parameters for adsorption of CO_2 in **PSIF-4a**. These parameters were determined by fitting adsorption isotherms for temperatures ranging from 263 K to 293 K.

Parameter	*Value*
$q_{sat,A}$	0.48 mol/kg
$q_{sat,B}$	1.85 mol/kg
b_{A0}	1.37×10^{-8} Pa^{-1}
E_A	31.9 kJ/mol
b_{B0}	6.4110^{-9} Pa^{-1}
E_B	26.2 kJ/mol

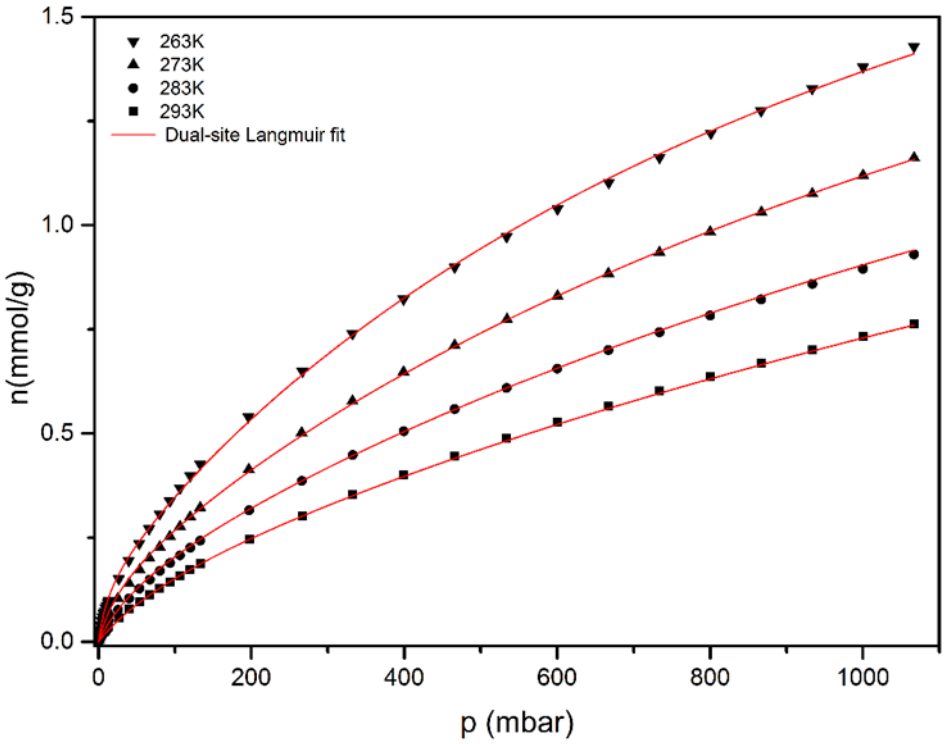

Figure S35. CO_2 isotherms for **PSIF-5a**.

Table S10. Dual-site Langmuir parameters for adsorption of CO_2 in **PSIF-5a**. These parameters were determined by fitting adsorption isotherms for temperatures ranging from 263 K to 293 K.

Parameter	*Value*
$q_{sat,A}$	0.16 mol/kg
$q_{sat,B}$	2.61 mol/kg
b_{A0}	3.11×10^{-10} Pa^{-1}
E_A	42.0 kJ/mol
b_{B0}	1.90×10^{-8} Pa^{-1}
E_B	23.5 kJ/mol

Section 4. I_2 Adsorption kinetic studies

The kinetic data was analyzed using pseudo-first-order and pseudo-second-order models. The pseudo-first-order model was given by Lagergren (eq 4):[9]

$$\ln(q_e - q_t) = \ln q_e - (\frac{k_1}{2.303})t \quad (4)$$

Where q_t(g/g) is the amount of I_2 adsorbed at time *t*, q_e is the adsorption capacity at equilibrium (g/g), k_1 is the pseudo-first-order rate constant (h^{-1}), and *t* is the adsorption time (h). The value of the adsorption rate constant, k_1, was determined from the plot of $\ln(q_e - q_t)$ versus *t*.
The pseudo-second-order model is expressed as the following linear equation (eq 5):

$$\frac{t}{q_t} = \frac{1}{k_2 \times q_e^2} + \frac{t}{q_e} \quad (5)$$

where k_2 is the pseudo-second-order rate constant ($g \times g^{-1} \times min^{-1}$). The value of k_2 and q_e can be determined by the plot of t/q_t versus *t*.

Table S11. Calculated parameters of pseudo-first-order and pseudo-second-order kinetic model of iodine uptake of PSIF as a function of time at 75 °C and ambient pressure.

	Pseudo-first-order kinetic model				Pseudo-second-order kinetic model		
	$q_{e,exp}$ [$g \times g^{-1}$] [a]	$q_{e,calc}$ [$g \times g^{-1}$] [b]	k_1 [h^{-1}]	R^2	$q_{e,calc}$ [$g \times g^{-1}$] [b]	k_2 [$g \times g^{-1} \times h^{-1}$]	R^2
PSIF-1a	4.851	4.727 ± 0.060	1.144 ± 0.091	0.9922	4.904 ± 0.006	0.4579 ± 0.0066	0.9999
PSIF-2a	3.460	3.283 ± 0.067	0.5036 ± 0.0499	0.9852	3.561 ± 0.009	0.1983 ± 0.0035	0.9999
PSIF-3a	4.110	4.154 ± 0.068	0.2651 ± 0.0185	0.9997	4.656 ± 0.216	0.0765 ± 0.0206	0.9941
PSIF-4a	2.440	2.323 ± 0.057	0.7451 ± 0.0960	0.9747	2.469 ± 0.021	0.4621 ± 0.0323	0.9999
PSIF-5a	3.014	2.954 ± 0.029	1.541 ± 0.114	0.9953	3.032 ± 0.010	1.222 ± 0.061	0.9999

[a] Equilibrium adsorption capacity from experiment.

[b] Equilibrium adsorption capacity calculated to kinetic models.

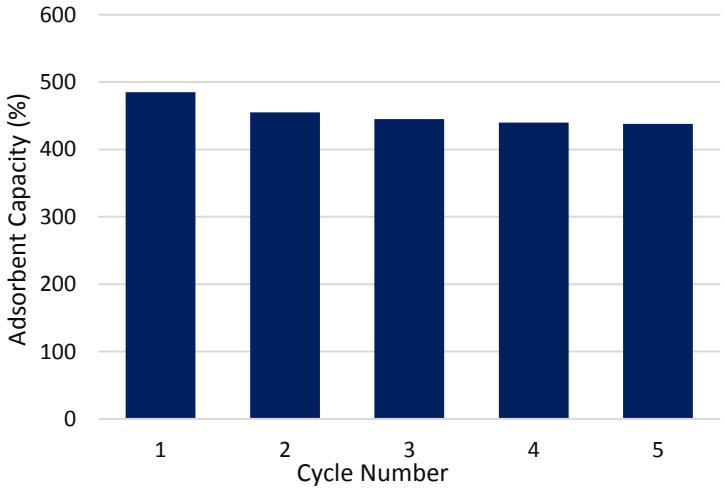

Figure S36. Recyclability of **PSIF-1a** for I_2 capture. A sample with initial I_2 uptake of 485%wt was used for the recycling test.

Table S12. Iodine uptake properties of porous materials.

	Adsorbent	*Iodine capacity (mgI_2/g)*	*References*
1	PSIF-1	4851	This work
2	SIOC-COF-7	4810	10
3	TTPB	4430	11
4	PSIF-3	4110	This work
5	POP-2	3820	12
6	PSIF-2	3460	This work
7	HCMP-3(reduced)	3360	13
8	CalP4-Li	3120	14
9	PSIF-5	3014	This work
10	AzoPPN	2900	15
11	BDP-CPP-1	2830	16
12	PAF-24	2760	17
13	PAF-23	2710	17
14	PAF-25	2600	17
15	PSIF-4	2440	This work
16	azo-Trip	2380	18
17	NiMoS chalcogels	2250	19
18	CMPN-3	2080	20
19	NiP-CMP	2020	21
20	PAF-1	1860	22
21	NTP	1800	23
22	Cu-BTC	1750	24
23	JUC-Z2	1440	22
24	UiO-66-PYDC	1250	25
25	ZIF-8	1200	26
26	CC3	364	27
27	Activated carbon	300	23
28	Ag@Zeolite Mordenites	275	28
29	Ag@Mon-POF	250	29
30	NOP-54	202	30

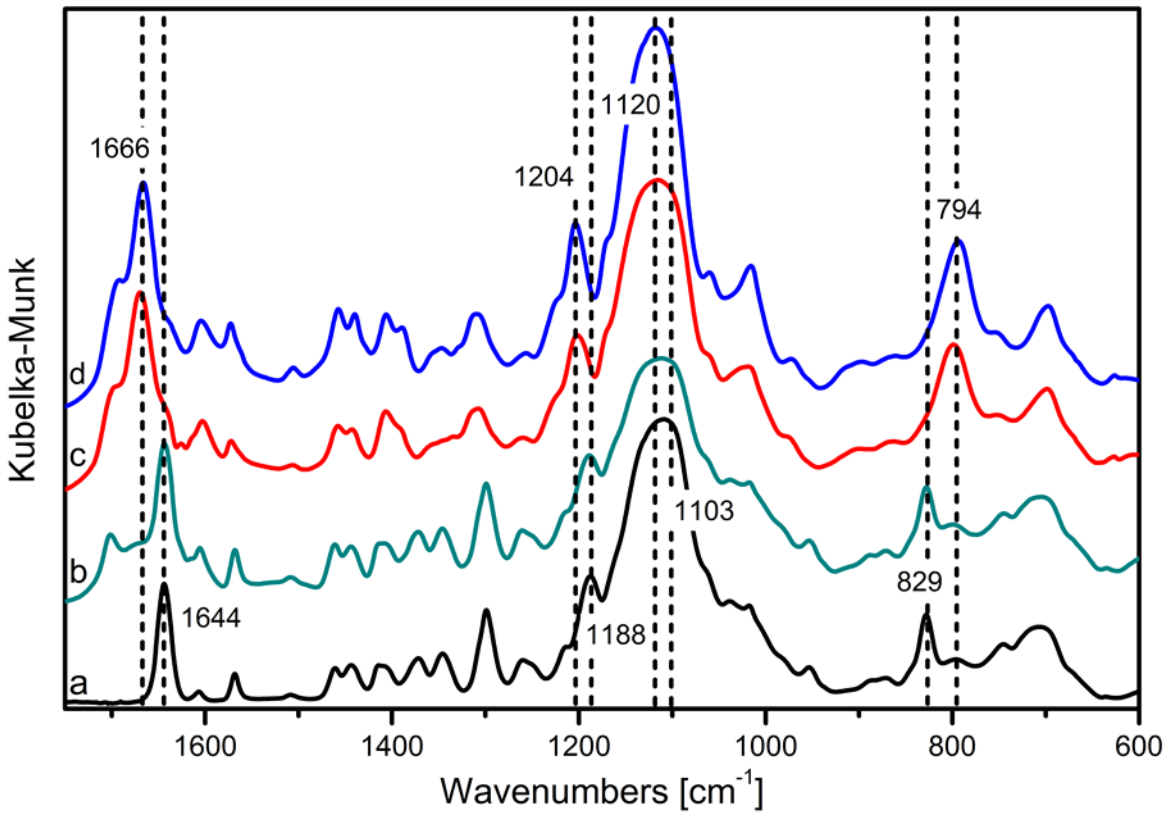

Figure S37. DRIFT spectra of **PSIF-1a** before (a) and after exposure to I_2 vapors during: 15 min (b); 1h (c); 15 h (d).

Section 5. I_2 desorption kinetic studies

1. TGA studies of PSIFs and I_2@PSIF

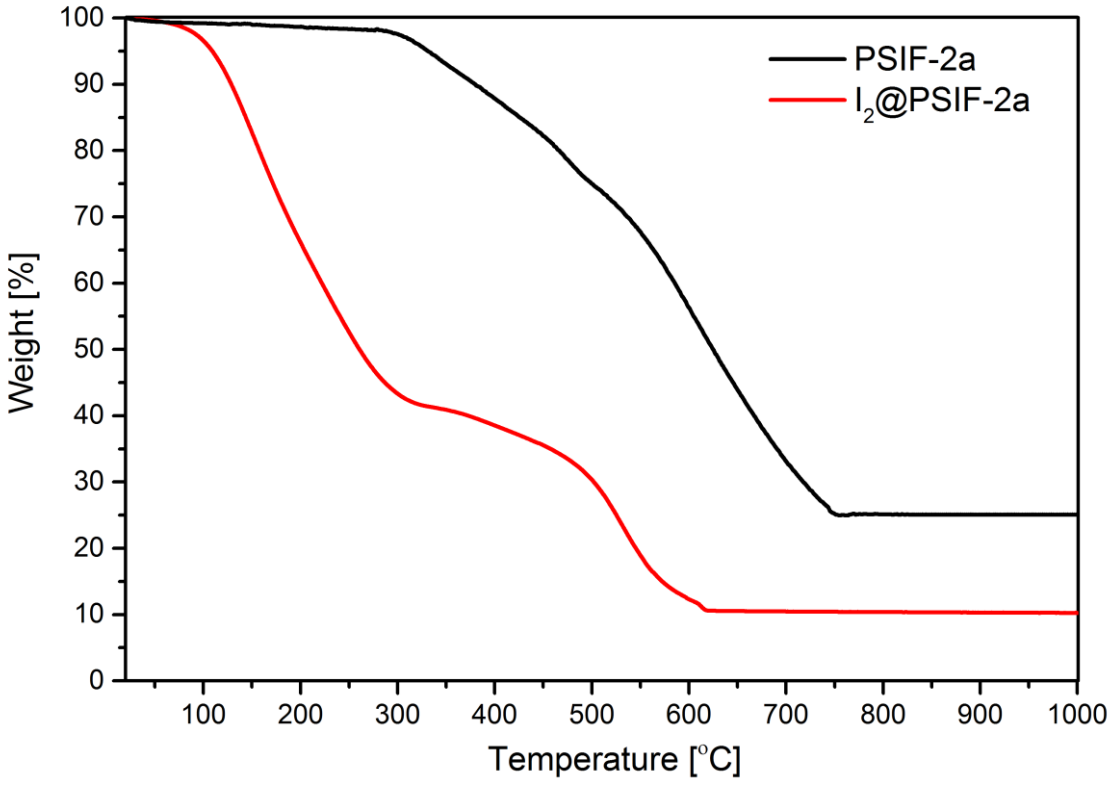

Figure S38. TGA trace of **PSIF-2a** and **I_2@PSIF-2a**.

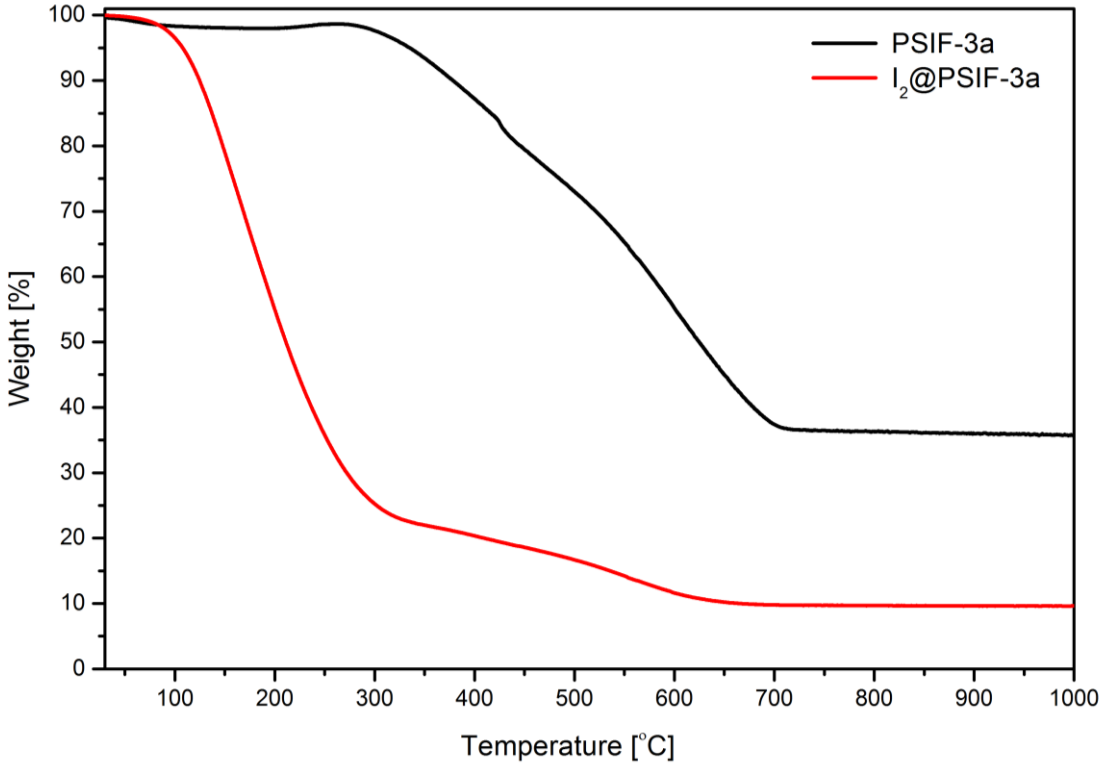

Figure S39. TGA trace of **PSIF-3a** and **I_2@PSIF-3a**.

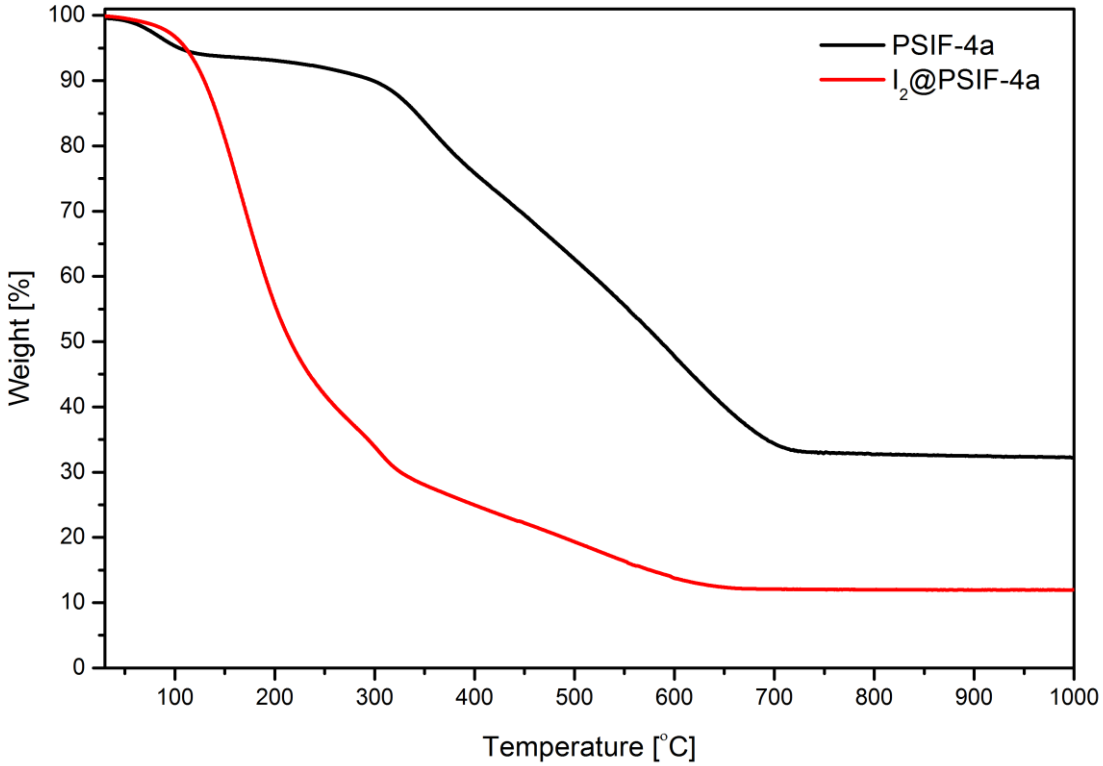

Figure S40. TGA trace of **PSIF-4a** and **I₂@PSIF-4a**.

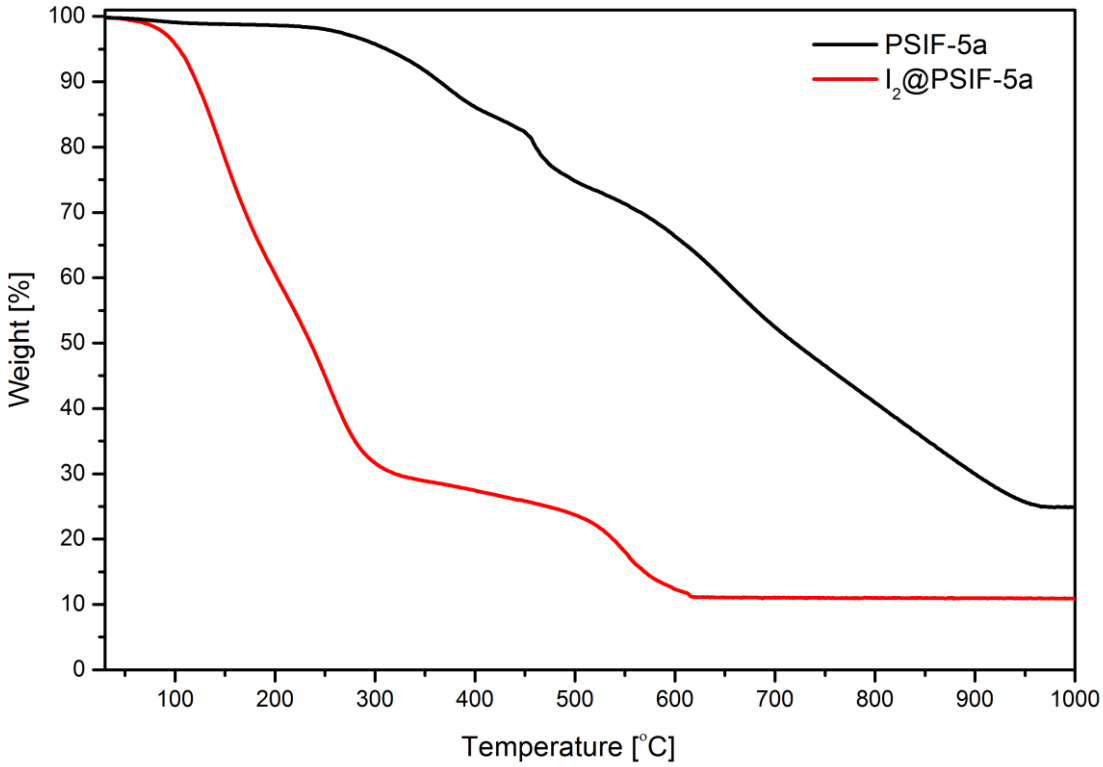

Figure S41. TGA trace of **PSIF-5a** and **I₂@PSIF-5a**.

2. Calculations of apparent activation energy of I_2 desorption

Delineation of E_{aa} was performed using the Kissinger method (eq 6):[31]

$$ln\left(\frac{\beta}{T_m^2}\right) = \frac{-E_{aa}}{RT_m} + const \quad (6)$$

where β is the heating rate, T_m is the temperature of iodine release.

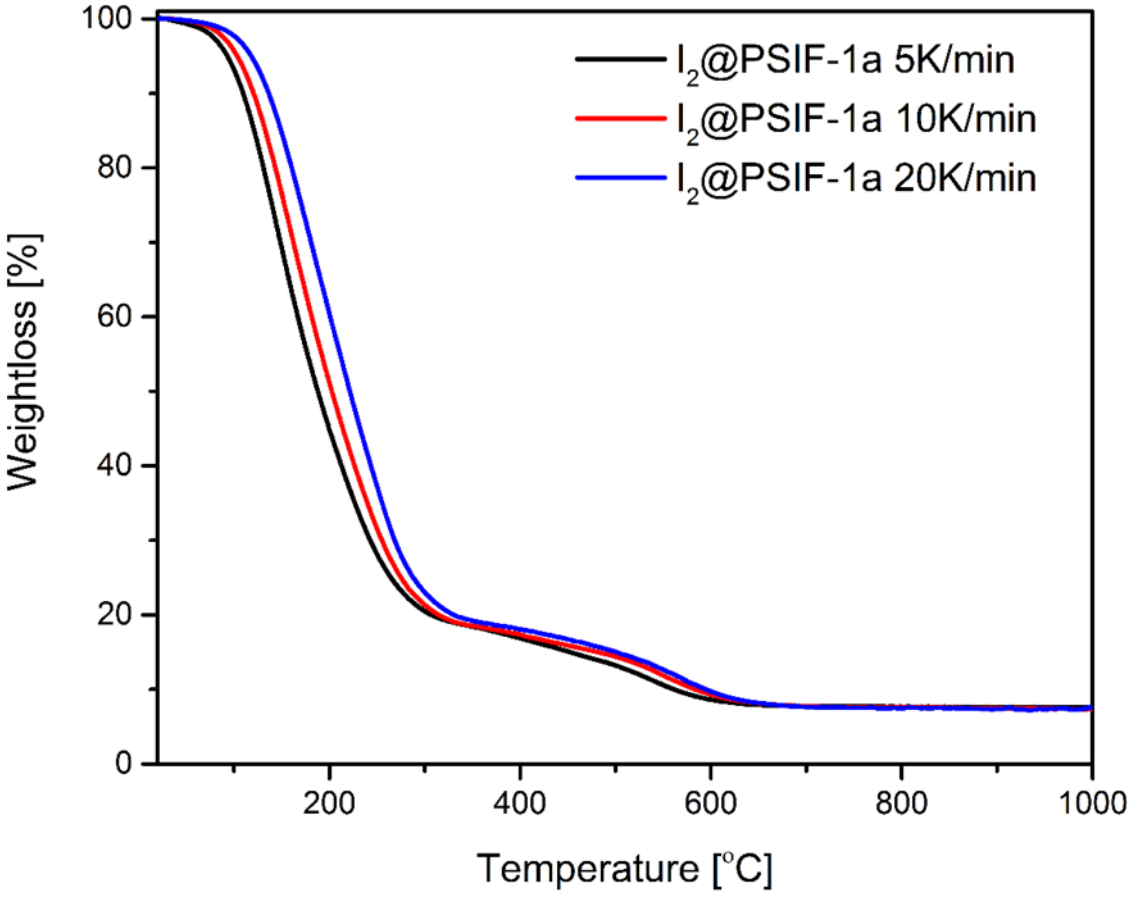

Figure S42. TGA profiles for **I_2@PSIF-1a** obtained at different heating rates.

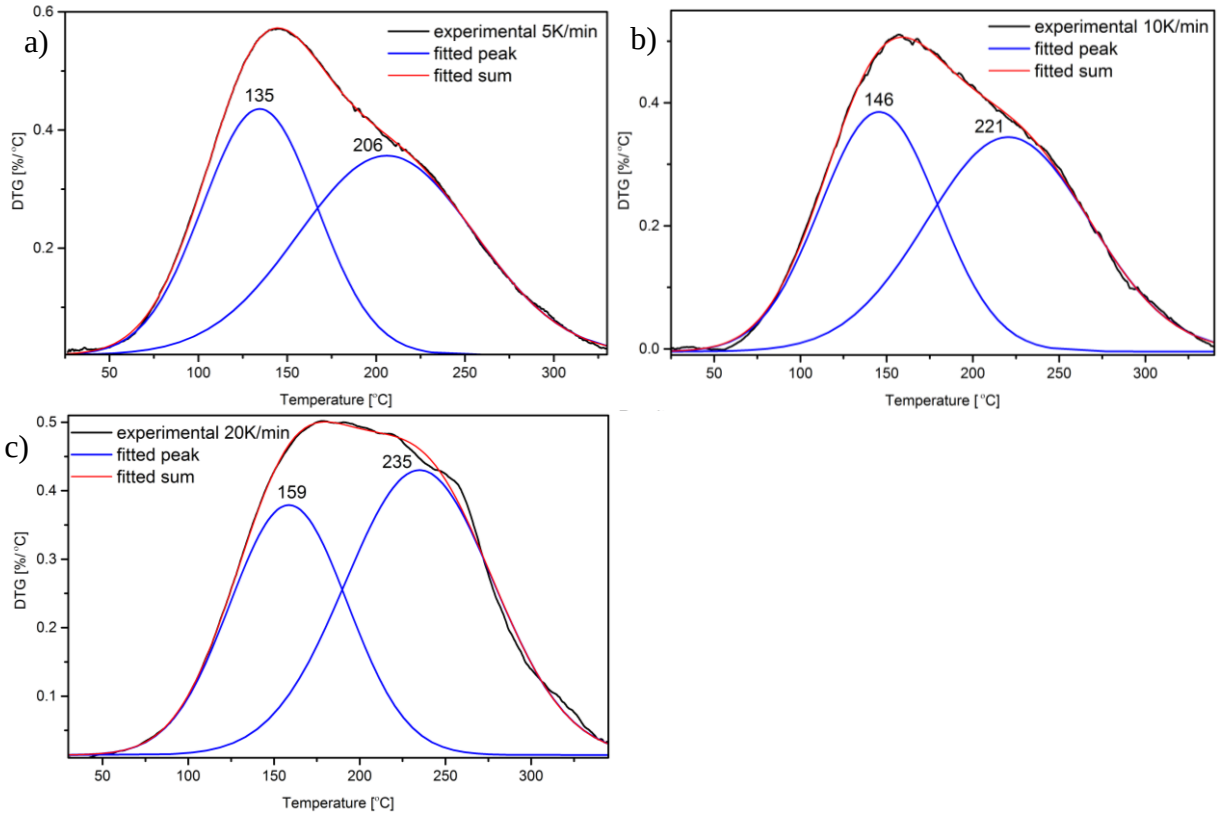

Figure S43. DTG curves for **I_2@PSIF-1a** obtained at different heating rates: a) 5 K/min, b) 10 K/min and c) 20 K/min.

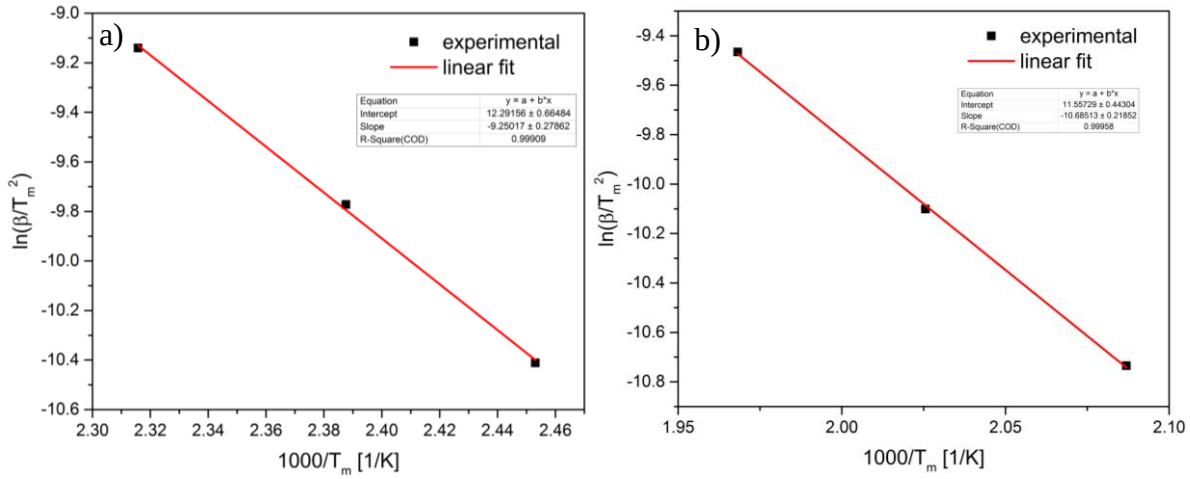

Figure S44. Plot of $\ln(\beta/T_m^2)$ versus $10^3/T_m$ used to calculate E_{aa} by Kissinger method a) first step; b) second step.

Literature

(1) Janeta, M.; John, Ł.; Ejfler, J.; Szafert, S. High-Yield Synthesis of Amido-Functionalized Polyoctahedral Oligomeric Silsesquioxanes by Using Acyl Chlorides. *Chem. – Eur. J.* **2014**, *20* (48), 15966–15974.

(2) Janeta, M.; John, Ł.; Ejfler, J.; Lis, T.; Szafert, S. Multifunctional Imine-POSS as Uncommon 3D Nanobuilding Blocks for Supramolecular Hybrid Materials: Synthesis, Structural Characterization, and Properties. *Dalton Trans.* **2016**, *45* (31), 12312–12321.

(3) Zhao, H.; Liao, J.; Ning, J.; Xie, Y.; Cao, Y.; Chen, L.; Yang, D.; Wang, B. Efficient Synthesis of Novel Bis(Dipyrromethanes) with Versatile Linkers via Indium(III) Chloride-Catalyzed Condensation of Pyrrole and Dialdehydes. *Adv. Synth. Catal.* **2010**, *352* (17), 3083–3088.

(4) Pandey, P.; Katsoulidis, A. P.; Eryazici, I.; Wu, Y.; Kanatzidis, M. G.; Nguyen, S. T. Imine-Linked Microporous Polymer Organic Frameworks. *Chem. Mater.* **2010**, *22* (17), 4974–4979.

(5) Chong, J. H.; Sauer, M.; Patrick, B. O.; MacLachlan, M. J. Highly Stable Keto-Enamine Salicylideneanilines. *Org. Lett.* **2003**, *5* (21), 3823–3826.

(6) Mitra, S.; Sasmal, H. S.; Kundu, T.; Kandambeth, S.; Illath, K.; Díaz Díaz, D.; Banerjee, R. Targeted Drug Delivery in Covalent Organic Nanosheets (CONs) via Sequential Postsynthetic Modification. *J. Am. Chem. Soc.* **2017**, *139* (12), 4513–4520.

(7) Zhao, Y.-C.; Wang, T.; Zhang, L.-M.; Cui, Y.; Han, B.-H. Facile Approach to Preparing Microporous Organic Polymers through Benzoin Condensation. *ACS Appl. Mater. Interfaces* **2012**, *4* (12), 6975–6981.

(8) Mason, J. A.; Sumida, K.; Herm, Z. R.; Krishna, R.; Long, J. R. Evaluating Metal–organic Frameworks for Post-Combustion Carbon Dioxide Capture via Temperature Swing Adsorption. *Energy Environ. Sci.* **2011**, *4* (8), 3030–3040.

(9) Lagergren, S. About the Theory of So-Called Adsorption of Soluble Substances. *K. Sven. Vetenskapsakademiens Handl.* **1898**, *24* (4), 1–6.

(10) Yin, Z.-J.; Xu, S.-Q.; Zhan, T.-G.; Qi, Q.-Y.; Wu, Z.-Q.; Zhao, X. Ultrahigh Volatile Iodine Uptake by Hollow Microspheres Formed from a Heteropore Covalent Organic Framework. *Chem. Commun.* **2017**.

(11) Geng, T.; Zhu, Z.; Zhang, W.; Wang, Y. A Nitrogen-Rich Fluorescent Conjugated Microporous Polymer with Triazine and Triphenylamine Units for High Iodine Capture and Nitro Aromatic Compound Detection. *J. Mater. Chem. A* **2017**, *5* (16), 7612–7617.

(12) Qian, X.; Wang, B.; Zhu, Z.-Q.; Sun, H.-X.; Ren, F.; Mu, P.; Ma, C.; Liang, W.-D.; Li, A. Novel N-Rich Porous Organic Polymers with Extremely High Uptake for Capture and Reversible Storage of Volatile Iodine. *J. Hazard. Mater.* **2017**, *338* (Supplement C), 224–232.

(13) Liao, Y.; Weber, J.; Mills, B. M.; Ren, Z.; Faul, C. F. J. Highly Efficient and Reversible Iodine Capture in Hexaphenylbenzene-Based Conjugated Microporous Polymers. *Macromolecules* **2016**, *49* (17), 6322–6333.

(14) Shetty, D.; Raya, J.; Han, D. S.; Asfari, Z.; Olsen, J.-C.; Trabolsi, A. Lithiated Polycalix[4]Arenes for Efficient Adsorption of Iodine from Solution and Vapor Phases. *Chem. Mater.* **2017**, *29* (21), 8968–8972.

(15) Li, H.; Ding, X.; Han, B.-H. Porous Azo-Bridged Porphyrin–Phthalocyanine Network with High Iodine Capture Capability. *Chem. – Eur. J.* **2016**, *22* (33), 11863–11868.

(16) Zhu, Y.; Ji, Y.-J.; Wang, D.-G.; Zhang, Y.; Tang, H.; Jia, X.-R.; Song, M.; Yu, G.; Kuang, G.-C. BODIPY-Based Conjugated Porous Polymers for Highly Efficient Volatile Iodine Capture. *J. Mater. Chem. A* **2017**, *5* (14), 6622–6629.

(17) Yan, Z.; Yuan, Y.; Tian, Y.; Zhang, D.; Zhu, G. Highly Efficient Enrichment of Volatile Iodine by Charged Porous Aromatic Frameworks with Three Sorption Sites. *Angew. Chem. Int. Ed.* **2015**, *54* (43), 12733–12737.
(18) Dang, Q.-Q.; Wang, X.-M.; Zhan, Y.-F.; Zhang, X.-M. An Azo-Linked Porous Triptycene Network as an Absorbent for CO_2 and Iodine Uptake. *Polym. Chem.* **2016**, *7* (3), 643–647.
(19) Subrahmanyam, K. S.; Sarma, D.; Malliakas, C. D.; Polychronopoulou, K.; Riley, B. J.; Pierce, D. A.; Chun, J.; Kanatzidis, M. G. Chalcogenide Aerogels as Sorbents for Radioactive Iodine. *Chem. Mater.* **2015**, *27* (7), 2619–2626.
(20) Chen, Y.; Sun, H.; Yang, R.; Wang, T.; Pei, C.; Xiang, Z.; Zhu, Z.; Liang, W.; Li, A.; Deng, W. Synthesis of Conjugated Microporous Polymer Nanotubes with Large Surface Areas as Absorbents for Iodine and CO_2 Uptake. *J. Mater. Chem. A* **2015**, *3* (1), 87–91.
(21) A, S.; Zhang, Y.; Li, Z.; Xia, H.; Xue, M.; Liu, X.; Mu, Y. Highly Efficient and Reversible Iodine Capture Using a Metalloporphyrin-Based Conjugated Microporous Polymer. *Chem Commun* **2014**, *50* (62), 8495–8498.
(22) Pei, C.; Ben, T.; Xu, S.; Qiu, S. Ultrahigh Iodine Adsorption in Porous Organic Frameworks. *J Mater Chem A* **2014**, *2* (20), 7179–7187.
(23) Ma, H.; Chen, J.-J.; Tan, L.; Bu, J.-H.; Zhu, Y.; Tan, B.; Zhang, C. Nitrogen-Rich Triptycene-Based Porous Polymer for Gas Storage and Iodine Enrichment. *ACS Macro Lett.* **2016**, *5* (9), 1039–1043.
(24) Sava, D. F.; Chapman, K. W.; Rodriguez, M. A.; Greathouse, J. A.; Crozier, P. S.; Zhao, H.; Chupas, P. J.; Nenoff, T. M. Competitive I_2 Sorption by Cu-BTC from Humid Gas Streams. *Chem. Mater.* **2013**, *25* (13), 2591–2596.
(25) Wang, Z.; Huang, Y.; Yang, J.; Li, Y.; Zhuang, Q.; Gu, J. The Water-Based Synthesis of Chemically Stable Zr-Based MOFs Using Pyridine-Containing Ligands and Their Exceptionally High Adsorption Capacity for Iodine. *Dalton Trans* **2017**.
(26) Sava, D. F.; Garino, T. J.; Nenoff, T. M. Iodine Confinement into Metal–Organic Frameworks (MOFs): Low-Temperature Sintering Glasses To Form Novel Glass Composite Material (GCM) Alternative Waste Forms. *Ind. Eng. Chem. Res.* **2012**, *51* (2), 614–620.
(27) Hasell, T.; Schmidtmann, M.; Cooper, A. I. Molecular Doping of Porous Organic Cages. *J. Am. Chem. Soc.* **2011**, *133* (38), 14920–14923.
(28) Chapman, K. W.; Chupas, P. J.; Nenoff, T. M. Radioactive Iodine Capture in Silver-Containing Mordenites through Nanoscale Silver Iodide Formation. *J. Am. Chem. Soc.* **2010**, *132* (26), 8897–8899.
(29) Katsoulidis, A. P.; He, J.; Kanatzidis, M. G. Functional Monolithic Polymeric Organic Framework Aerogel as Reducing and Hosting Media for Ag Nanoparticles and Application in Capturing of Iodine Vapors. *Chem. Mater.* **2012**, *24* (10), 1937–1943.
(30) Chen, D.; Fu, Y.; Yu, W.; Yu, G.; Pan, C. Versatile Adamantane-Based Porous Polymers with Enhanced Microporosity for Efficient CO_2 Capture and Iodine Removal. *Chem. Eng. J.* **2018**, *334* (Supplement C), 900–906.
(31) Blaine, R. L.; Kissinger, H. E. Homer Kissinger and the Kissinger Equation. *Thermochim. Acta* **2012**, *540*, 1–6.